JOURNAL OF GEOPHYSICAL RESEARCH, VOL. 89, NO. D3, PAGES 4841–4872, JUNE 20, 1984

The Vertical Distribution of Ozone in the Mesosphere and Lower Thermosphere

MARK ALLEN,[1] JONATHAN I. LUNINE, and YUK L. YUNG

Division of Geological and Planetary Sciences, California Institute of Technology

An assessment is made of the ability of current theory to explain the phenomenology of upper atmospheric ozone as revealed by the sizeable body of measurements presently available. The chemistry of ozone in the mesosphere and lower thermosphere is closely coupled to the chemistries of other oxygen/hydrogen-containing species, which must be considered concurrently. To provide insight into the sensitivity of model calculations to the choice of values used for key chemical rate constants and climatological parameters, simple analytical expressions for ozone are derived for those situations when it is in photochemical steady state, the mesosphere during daylight hours and the lower thermosphere throughout the full diurnal period. The model is found to reproduce the detailed Aladdin 74 rocket measurements of ozone from 50 to 95 km, numerous other measurements of mid-latitude ozone in the lower mesosphere, the secondary maximum in the ozone vertical distribution at the mesopause, and the diurnal variability of ozone seen in the radio measurements of Wilson and Schwartz (1981) and other observations. The agreement with the Aladdin 74 data results from adjusting some key parameters within the uncertainties of laboratory measurements or known natural climatological variability. The variety of mid-latitude observations can be understood in terms of the estimated variability of environmental factors: diurnal, seasonal, and solar cycles in the solar illumination; the abundance of water vapor; and the details of the thermal profile of the atmosphere. The ozone secondary maximum results from the onset of the coupling between active-hydrogen and active-oxygen chemistry and its observed variability may be a consequence of secular changes in mesopause dynamics. Above ~95 km, ozone observations are consistently higher than model results and cannot be accounted for by the set of reactions currently included in the model.

INTRODUCTION

Ozone in the terrestrial atmosphere between the stratopause (~50 km altitude) and the homopause (~100 km altitude), encompassing the mesosphere and lower thermosphere, is a subject worthy of detailed study, because its presence is a key factor in upper atmospheric processes that are of significant importance to human activities and the evolution of the terrestrial ecosystem. As a result of its optical and chemical properties, ozone affects the thermal structure and dynamics of the upper atmosphere [*London*, 1980] and its state of ionization, particularly in the *D* region where negative ions are important [*Chamberlain*, 1978]. Thus, the behavior of upper atmospheric ozone is ultimately associated with such diverse phenomena as the operations of low earth-orbit satellites (as in the case of the premature fall of Skylab) [*National Academy of Sciences*, 1981] (NAS), the chemical evolution of the whole atmosphere on geological times [*Hunten and Strobel*, 1974; *Liu and Donahue*, 1974*a*, *b*; *Hunten and Donahue*, 1976], the upper stratospheric ozone layer (and the viability of biological activity on the surface of the earth) [*Hudson and Reed*, 1979], and clarity in long range communications [*NAS*, 1981]. Since at least one region of the solar spectrum that is known to influence the distribution of ozone in the mesosphere has been observed to vary over the course of the 27-day solar rotation [*Rottman et al.*, 1982] and the 11-year solar cycle [*Mount et al.*, 1980; *Mount and Rottman*, 1981; *Rottman*, 1981], ozone is associated with a clearly established coupling between solar variability and terrestrial phenomena.

An understanding of the ozone chemistry above the stratopause can be of great assistance to the larger program of stratospheric ozone research because high altitude ozone is affected by some of the same chemical cycles that are important in controlling stratospheric ozone [*World Meteorological Organization*, 1981] (WMO). Since a smaller group of reactions is sufficient for describing the behavior of mesospheric ozone, there is an opportunity to test key parts of stratospheric models under the simplified conditions of the upper atmosphere. This is important because current stratospheric models with fully updated kinetic rate constants underestimate the observed ozone distribution between 35 and 50 km [*Ko and Sze*, 1983; L. Froidevaux, private communication, 1983], but the cause of this deficit is unclear due to the difficulty in assessing the effects of any particular catalytic cycle for ozone loss in the stratosphere.

Such are the motivations for trying to understand in detail the behavior of ozone in the mesosphere and lower thermosphere. While much is known about the stratosphere and upper thermosphere, there is in general surprisingly little data on the chemical composition in the intervening atmosphere because this altitude range is too high for effective use of stratospheric measurement techniques and too low for in situ satellite measurements [*NAS*, 1981]. However, in the case of ozone, detection is relatively easy and it has been monitored by ground-based telescopes [for example, *Wilson and Schwartz*, 1981], by in situ rocket measurements [for example, *Weeks et al.*, 1978], and from

[1] Also at Earth and Space Sciences Division, Jet Propulsion Laboratory.

Paper number 3D1922.
0148-0227/84/003D-1922$05.00

satellites [*Krueger et al.*, 1980]. Increasingly sophisticated models of mesospheric/lower thermospheric ozone chemistry have been published in the past decade. *Nicolet* [1971, 1980] has presented the set of reactions important for the hydrogen/oxygen chemistry. The papers by *Hunt* [1971, 1973], *Thomas and Bowman* [1972], *Whitten and Turco* [1974], *Kosheleν* [1976], *Moreels et al.* [1977], *Logan et al.* [1978], *Keneshea et al.* [1979], *Crutzen and Solomon* [1980], *Wang et al.* [1981], *Battaner and Rodrigo* [1981], *Rusch and Liu* [1981], *Prather* [1981], *Garcia and Solomon* [1983], and *Solomon et al.* [1983] all present model profiles of ozone for part or all of the altitude range between the stratopause and the homopause. As a result of this cumulative work, a general understanding of the key chemical and atmospheric parameters affecting the ozone distribution has developed. Some of these papers present limited comparisons between model distributions and the observations available at the time. Since most of this work appeared, there have been significant changes in important reaction rate constants and improvements in the calculations of radiative transfer in the upper atmosphere and the treatment of relevant background atmosphere parameters. Moreover, in recent years the quantity and quality of ozone observational data has significantly improved, allowing more definitive intercomparisons between measurements and models. Thus, a new study benefitting from this recent progress seemed warranted with the purpose of identifying remaining shortcomings in our understanding of upper atmospheric ozone. In this paper the particular focus will be on the details of the vertical distribution of ozone and the diurnal and other naturally occurring variations in the ozone distribution at mid-latitudes.

The work presented in this paper is part of a larger research program focused on using observational data in conjunction with model calculations specific to the circumstances of the observations to derive values for the physical properties of the mesosphere and lower thermosphere and to test proposed reaction mechanisms of importance to the aeronomy of this altitude range. The first phase of this program was presented in *Allen et al.* [1981] (hereinafter Paper I). In this paper, we reported the derivation of values for vertical eddy diffusion that are consistent with the altitude distribution of several long-lived trace species. Preliminary results from our ozone modeling were used to constrain the values for eddy diffusion near the mesopause. In the course of the work reported in Paper I, we found that key hydrogen/oxygen reaction rate constants had to be varied from the experimental values. Only briefly discussed in Paper I, these points are more fully developed in the current work.

We begin our considerations of upper atmospheric ozone with a review of the chemical processes affecting its vertical distribution. Simple analytical expressions for the ozone concentrations at different altitudes are derived which approximate the key elements of the ozone chemistry. These equations provide simple explanations of the sensitivity of model computations to the choice of rate constants and climatological parameters. In light of this understanding, we compare our model calculations with a detailed measurement of an ozone profile and refine some of our model parameters within the limits allowed by the uncertainties in their values. Our model so modified is used to assess the variation in ozone expected to result from perturbations in key climatological parameters. These predictions are then compared with the variability observed in the large accumulated body of mid-latitude measurements to verify our model description of ozone processes in the upper atmosphere.

CHEMISTRY OF OZONE IN THE UPPER ATMOSPHERE

To understand the chemical behavior of ozone in the mesosphere and lower thermosphere, one must simultaneously consider the chemistry of several compounds containing oxygen and/or hydrogen atoms. In particular, ozone is one of three important active-oxygen species, the others being atomic oxygen and the hydroxyl radical. These species result from breaking O-O bonds and are collectively destroyed when O-O bonds are reformed [cf. *DeMore and Yung*, 1982]. Considering this group of species together is similar to the odd-oxygen concept used in modeling stratospheric chemistry [*Johnston and Podolske* 1978; *Chang and Duewer*, 1979]. The cycling between O, O_3, and OH and the recycling of active-oxygen back to the inactive-oxygen reservoir, O_2, is affected by the presence of active-hydrogen species, H, OH, and HO_2. The abundance of these species relative to each other and the recycling between active-hydrogen and the inactive-hydrogen reservoirs, H_2O and H_2 (and in a minor way H_2O_2), must be understood to explain in turn the distribution of ozone. Analysis in terms of the behavior of active- and inactive-oxygen and hydrogen is employed in this paper only for the purposes of clarifying the net processes affecting ozone. The numerical calculations were performed by solving the full continuity equation, including transport, for each atomic and molecular species.

The important chemical reactions affecting the distribution of O_3 above the stratopause, as determined by decades of research, are listed in Table 1. This group of reactions is a subset of that used in Paper I. The concepts of active-oxygen and active-hydrogen to be utilized shortly are illustrated in the table by noting the net production or loss in active-O and/or active-H that results from each reaction [cf., *Johnston and Podolske*, 1978, Table 3]. In the next section, we will show how well this reaction scheme can reproduce a detailed observational O_3 profile with some modification of reaction rate constants. A full discussion of the values chosen for the rate constants is saved for then. Not included in Table 1 are reactions involving molecules that have nitrogen and/or halogen atoms, reactions that are known to be important for understanding ozone chemistry in the stratosphere [*WMO*, 1981, and references therein]. This omission is valid because the combined importance of nitrogen- and chlorine-catalyzed destruction of O_3 is less than 10-15% of the total O_3 loss rate at 50 km [*Frederick*, 1980; *WMO*, 1981] and less than 1% at 55 km [*Frederick*, 1980].

Most recently, *Thomas et al.* [1980], *Barth* [1981], and *Prather* [1981] review the key reaction cycles affecting ozone above the stratopause. An extensive discussion of the continuity equation for the important active-oxygen and active-hydrogen species in the mesosphere has been presented by *Nicolet* [1971, 1980]. In this section we will give a more qualitative overview of ozone chemistry and

TABLE 1. Important Reactions For Ozone Above The Stratopause

Reaction	Rate Constant[a]	Reference[b]	Net Production (>0) or Loss (<0)	
			Active-O	Active-H
(R1) $O_2 + h\nu \rightarrow 2O$	8.4×10^{-10}, 3.2×10^{-8c} $1775 \leq \lambda \leq 2560$ Å	*Watanabe* [1958]; *Hudson* [1974]; *Hudson and Reed* [1979]; *Prather* [1981]; *Allen and Frederick* [1982]	+2	0
(R2) $O_2 + h\nu \rightarrow O + O(^1D)$	1.5×10^{-13}, 1.6×10^{-7} $\lambda \leq 1775$ Å	*Watanabe* [1958]; *Ackerman* [1971]; Carver et al. [1977]; *Allen and Frederick* [1982]	+2	0
(R3) $O_3 + h\nu \rightarrow O_2 + O$	8.0×10^{-4}, 8.4×10^{-4d} $2000 \leq \lambda \leq 7300$ Å	*Ackerman* [1971]; *Hudson and Reed* [1979]; *DeMore et al.* [1981]	0	0
(R4) $O_3 + h\nu \rightarrow O_2 + O(^1D)$	5.1×10^{-3}, 5.5×10^{-3} $1675 \leq \lambda \leq 3200$ Å	*Ackerman* [1971]; *Hudson and Reed* [1979]; *DeMore et al.* [1981]	0	0
(R5) $H_2O + h\nu \rightarrow H + OH$	1.7×10^{-8}, 2.9×10^{-6} $\lambda \leq 2025$ Å	*Watanabe* [1958]; *Hudson* [1971]; *CIAP* [1975]; *Frederick and Hudson* [1980]; *T. G. Slanger* (private communication, 1981)	+1	+2
(R6) $H_2O + h\nu \rightarrow H_2 + O(^1D)$	6.4×10^{-12}, 1.8×10^{-6} $\lambda = 1215.7$ Å	*Frederick and Hudson* [1980]; *T. G. Slanger* (private communication, 1981)	+1	0
(R7) $H_2O_2 + h\nu \rightarrow 2OH$	7.0×10^{-5}, 8.0×10^{-5} $1220 \leq \lambda \leq 3500$ Å	*Schürgers and Welge* [1968]; *CIAP* [1975]; *DeMore et al.* [1981]	+2	+2
(R8) $O(^1D) + O_2 \rightarrow O + O_2$	$3.2 \times 10^{-11} e^{117/T}$	see text	0	0
(R9) $O(^1D) + N_2 \rightarrow O + N_2$	$1.8 \times 10^{-11} e^{157/T}$	see text	0	0
(R10) $O(^1D) + H_2O \rightarrow 2OH$	$2.3 \times 10^{-10} e^{-100/T}$	see text	+1	+2
(R11) $O(^1D) + H_2 \rightarrow H + OH$	1.1×10^{-10}		0	+2
(R12) $2O + M \rightarrow O_2 + M$	$9.59 \times 10^{-34} e^{480/T}$	*Logan et al.* [1978]	−2	0
(R13) $O + O_2 + O \rightarrow O_3 + O$	$2.15 \times 10^{-34} e^{345/T}$	see text	0	0
(R14) $O + O_2 + O_2 \rightarrow O_3 + O_2$	$2.15 \times 10^{-34} e^{345/T}$	*Klais et al.* [1980]; see text	0	0
(R15) $O + O_2 + N_2 \rightarrow O_3 + N_2$	$8.82 \times 10^{-35} e^{575/T}$	*Klais et al.* [1980]; see text	0	0
(R16) $O + O_3 \rightarrow 2O_2$	$1.5 \times 10^{-11} e^{-2218/T}$		−2	0
(R17) $O + OH \rightarrow O_2 + H$	$2.3 \times 10^{-11} e^{-90/T}$	see text	−2	0
(R18) $O + HO_2 \rightarrow OH + O_2$	$2.8 \times 10^{-11} e^{172/T}$	see text	0	0
(R19) $O + H_2O_2 \rightarrow OH + HO_2$	$1.0 \times 10^{-11} e^{-2500/T}$		0	+2
(R20) $O + H_2 \rightarrow OH + H$	$1.6 \times 10^{-11} e^{-4570/T}$	*Hampson* [1980]	0	+2
(R21) $OH + O_3 \rightarrow HO_2 + O_2$	$1.6 \times 10^{-12} e^{-940/T}$		−2	0
(R22) $2OH \rightarrow H_2O + O$	$4.5 \times 10^{-12} e^{-275/T}$	*WMO* [1981]	−1	−2
(R23) $OH + HO_2 \rightarrow H_2O + O_2$	8.4×10^{-11}	see text	−1	−2
(R24) $OH + H_2O_2 \rightarrow H_2O + HO_2$	$2.9 \times 10^{-12} e^{-160/T}$	*W. B. DeMore* (private communication, 1982)	−1	0
(R25) $OH + H_2 \rightarrow H_2O + H$	$7.7 \times 10^{-12} e^{-2100/T}$	*W. B. DeMore* (private communication, 1982)	−1	0
(R26) $HO_2 + O_3 \rightarrow OH + 2O_2$	$1.4 \times 10^{-14} e^{-580/T}$		0	0
(R27) $2HO_2 \rightarrow H_2O_2 + O_2$	$2.4 \times 10^{-14} e^{1250/T}$	*S. P. Sander* (private communication, 1982)	0	−2
(R28) $H + O_2 + M \rightarrow HO_2 + M$	$1.76 \times 10^{-28} T^{-1.4}$	see text	0	0
(R29) $H + O_3 \rightarrow OH + O_2$	$1.4 \times 10^{-10} e^{-270/T}$	see text	0	0
(R30) $H + HO_2 \rightarrow H_2 + O_2$	6.0×10^{-12}	see text	0	−2
(R31) $H + HO_2 \rightarrow 2OH$	7.0×10^{-11}	see text	+2	0
(R32) $H + HO_2 \rightarrow H_2O + O$	2.3×10^{-12}	see text	+1	−2
(R33) $2H + M \rightarrow + H_2 + M$	$1.0 \times 10^{-30} T^{-0.8}$	*Trainor et al.* (1973)	0	−2
(R35) $CH_4 + OH \rightarrow CO + OH + 2H_2O$	$2.4 \times 10^{-12} e^{-1710/T}$	see Paper I	0	0
(R36) $CH_4 + O \rightarrow CO + 2OH + H_2O$	$3.5 \times 10^{-11} e^{-4550/T}$	see Paper I	+1	+2
(R37) $CH_4 + O(^1D) \rightarrow CO + 2OH + H_2O$	1.4×10^{-10}	see Paper I	+1	+2

[a] Photodissociation rate constants are in units of s^{-1}, two body rate constants in units of $cm^3\ s^{-1}$, three body rate constants in units of $cm^6\ s^{-1}$.

[b] Rate constants come from *DeMore et al.* [1982], unless otherwise noted.

[c] Diurnally averaged photodissociation values for 60 and 100 km, respectively, at summer solstice, 38°N latitude, using solar minimum flux [*Rottman*, 1981]. Indicated also is the wavelength range in which the cross sections are significant.

[d] Omitted from the discussion in Paper I was the fact that O_3 photolysis is increased by $1.9 \times 10^{-4}\ s^{-1}$ (diurnally averaged value) at all altitudes to account for the contribution of the Chappius bands in the visible [*CIAP*, 1975].

derive simple analytical expressions, where possible, to be used to predict the O_3 distribution in terms of parameters that are easy to determine. This also allows identification of the sensitivity of O_3 vertical and diurnal profiles to certain factors. In the following section, the sensitivity analysis will be used to identify key rate constants which, if revised, would allow better agreement between model results and observations. The suggested changes to the rate constant values will be compared with recent experimental results.

Using the reactions and rate constants listed in Table 1 and the atmospheric and computer models described in Paper I, a diurnal calculation was performed (comparable to model 2 of Paper I). The most important reactions for cycling among active-O species and interchange between active-and inactive-O are pictured in Figure 1. Some of the properties of these species culled from the results of the

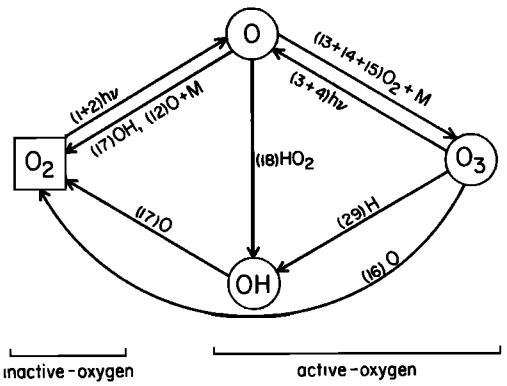

Fig. 1. Important reactions for recycling among active-oxygen species and for conversion from active-oxygen to inactive-oxygen and vice versa. Numbers in parentheses are reaction indices of Table 1.

aforementioned diurnal calculation are illustrated in Figure 2. Shown in Figure 2*a* are the chemical lifetimes at noon and midnight of O, O_3, and the active-oxygen group treated as a single entity. These are compared with the time scale for eddy diffusive transport. The consequent time-varying apportionment of active-O between O and O_3 is displayed in Figure 2*b*. As was discussed in Paper I, transport can directly affect the distribution of a species when its chemical lifetime is comparable to the mass transport time scale. When the chemical time scale is very short (up to ~1 hour), the diurnal behavior of the particular species is driven by the changing solar zenith angle. When in addition the production and loss terms balance, the species is in photochemical steady state and transport is not important. However, mass transport indirectly does affect these latter species when their chemistry involves longer-lived species controlled by transport (as will be seen, an important effect for O_3).

In the thermosphere (≳85 km), the lifetime of atomic O is consistently longer than 1 day throughout the diurnal cycle (Figure 2*a*). On the other hand, O_3 is always extremely short-lived (~10 minutes). As a consequence, active-O is predominantly atomic O (Figure 2*b*). If the lifetimes of all active-O species were short, the time scale for conversion of active-O to O_2 would be greater than the lifetime of any of the individual active-O species. In the thermosphere, the active-O group concept is not fully operative because of the long chemical lifetime of active-O, with the result that the lifetime of active-O is approximately equal to (actually slightly less than) that of atomic O. In these circumstances diurnal calculations cannot be performed by adopting active-O as a single species with subsequent partitioning among the group constituents by equilibrium considerations. As a result of the relative lifetimes of O and O_3 in the thermosphere, O_3 behaves as an active-O tracer in equilibrium with atomic O. Since the atomic O distribution is affected by eddy diffusion (Figure 2*a* and Paper I), then the O_3 profile will also be sensitive to mass transport rates.

At the mesopause (~80 km), there is a significant transformation of the active-O chemical cycle. In the mesosphere, active-O as a group becomes short-lived (and therefore the cycling among the group constituents very rapid) during daylight hours with the nature of the dominant species dependent on the exact altitude. At night below ~75 km, active-O is long-lived (~one day) but now O_3 is the dominant component (Figure 2*b*).

Analytical Expressions for the O_3 Abundance

When the lifetime of O_3 is relatively short and the production and loss terms nearly in balance, simple analytical expressions describing the time variability of the O_3 concentration can be derived assuming that O_3 is in photochemical

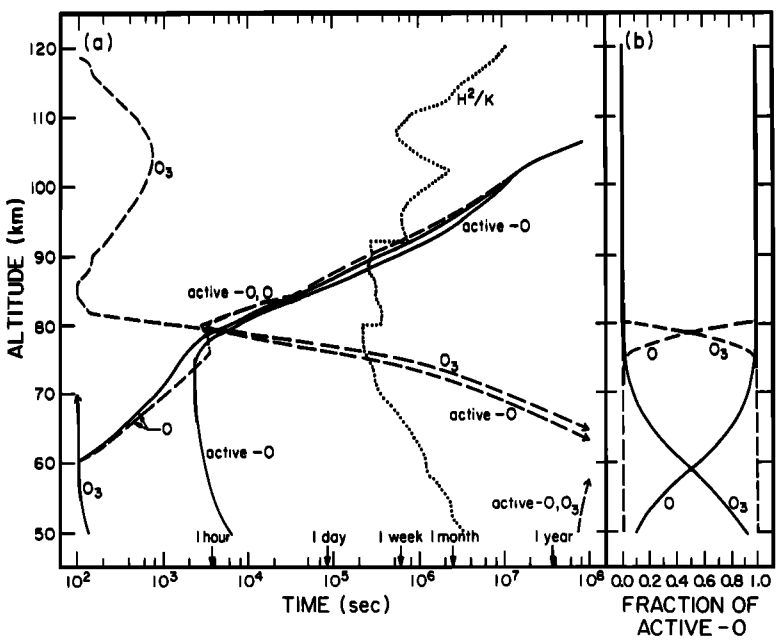

Fig. 2. Active-oxygen species above the stratopause. (*a*) Chemical lifetimes at noon (solid lines) and midnight (dashed lines) compared with eddy diffusion time scale (H_2/K). (*b*) The relative fraction of active-oxygen as atomic O and O_3 at noon (solid lines) and midnight (dashed lines).

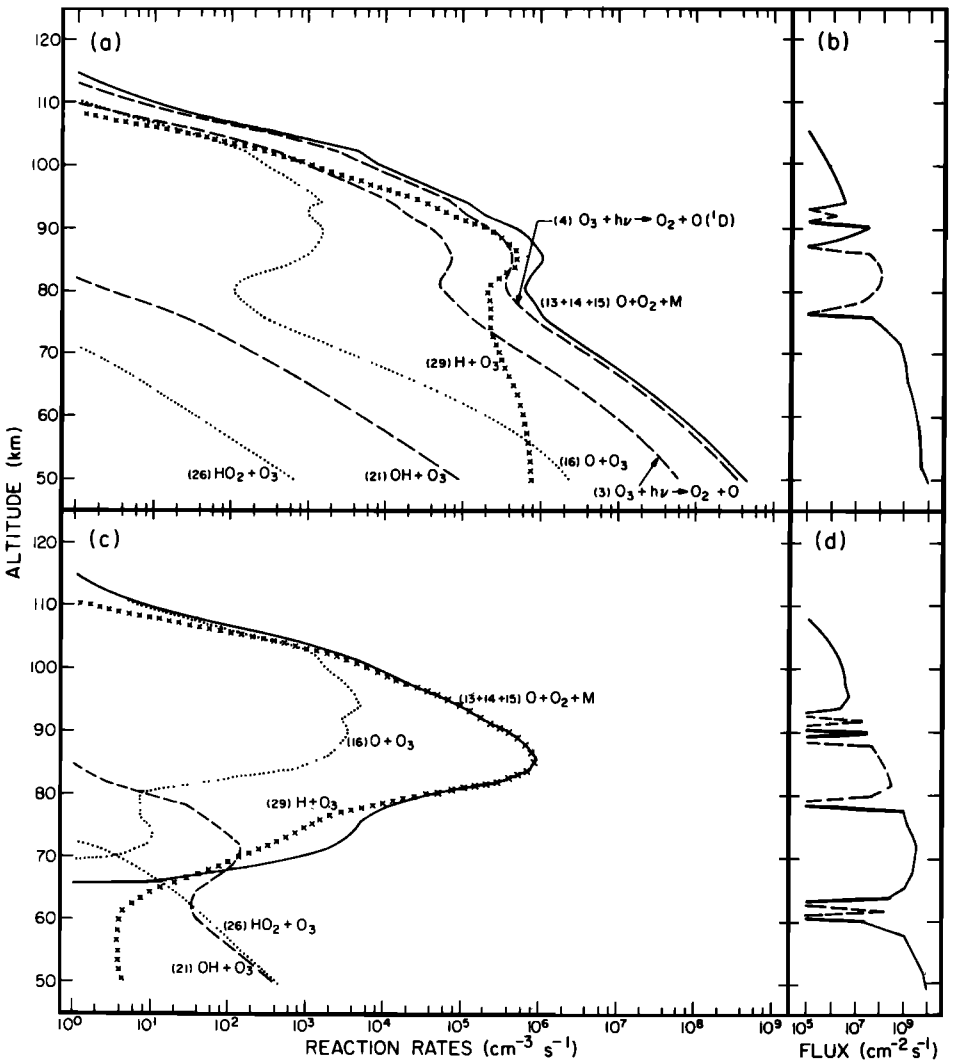

Fig. 3. Ozone chemistry. The rates of reactions important for the production and loss of O_3 at (*a*) noon and (*c*) midnight. The vertical transport of O_3 at (*b*) noon and (*d*) midnight (upward flux: solid lines; downward flux: dashed lines).

steady state. Such equations are most useful if the O_3 concentration is expressed in terms of the background abundances of long-lived species and measurable physical parameters. (Previously, *Bates and Nicolet* [1950] presented such an analysis for a pure oxygen atmosphere only.) We shall now derive analytical expressions for the daylight period below 80 km and for the full diurnal cycle above 80 km, as these are situations in which O_3 chemistry satisfies the conditions of photochemical steady state.

Shown in Figure 3 are the reactions most important for producing and destroying O_3. The rates of these reactions (and some less important ones) are presented in Figures 3*a* and 3*c* for noon and midnight, respectively. Figures 3*b* and 3*d* give the resulting values for vertical O_3 transport to show the relative importance of local chemistry and transport. Only one reaction is known to be significant for producing O_3 in the terrestrial atmosphere:

$$\text{(R13-R15)} \qquad O + O_2 + M \rightarrow O_3 + M$$

where M signifies a catalytic third body. (The *Rn* numbers refer to the identifying reaction index in Table 1.) During the day, photodissociation of O_3 ((R3) and (R4)) is an important destruction mechanism. Chemical loss of O_3 is predominantly due to reaction with atomic hydrogen,

$$\text{(R29)} \qquad H + O_3 \rightarrow OH + O_2$$

but, below 55 km and above ~105 km, the atomic O/atomic H ratio becomes sufficiently large that reaction with atomic oxygen,

$$\text{(R16)} \qquad O + O_3 \rightarrow 2O_2$$

is also an important O_3 loss channel. Thus, a general expression for the ozone distribution during periods of photochemical steady state is

$$[O_3] = \frac{[O][O_2](k_{13}[O] + k_{14}[O_2] + k_{15}[N_2])}{J_3 + J_4 + k_{29}[H] + k_{16}[O]} \qquad (1)$$

where the square brackets indicate concentration and each of the physical parameters and chemical abundances may

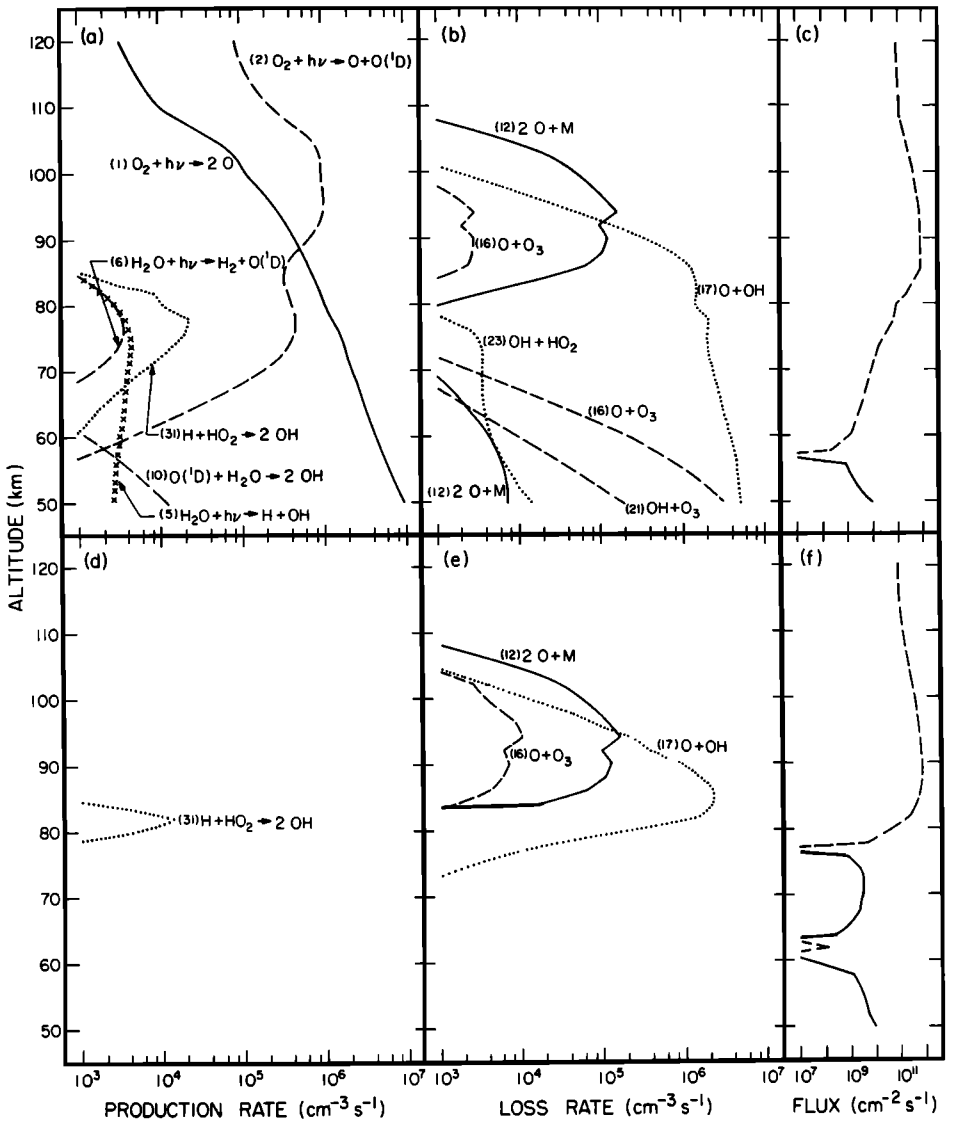

Fig. 4. Active-oxygen chemistry. The rates of production and loss of active-O at noon, (*a*) and (*b*), respectively, and at midnight, (*d*) and (*e*). The vertical transport of active-O at (*c*) noon and at (*f*) midnight (upward flux: solid lines; downward flux: dashed lines).

be a function of space and time. Photolytic rate constants are indicated by J_n and kinetic rate constants by k_n.

At 50 km, the daylight O_3 distribution will reflect the local nature of the background atmosphere (the O_2 and N_2 densities). The temporal variability will arise from the diurnal changes in the photodissociation rate constants directly (affecting the partitioning among active-O species) and indirectly by controlling the abundance of active-O and active-H, both of which are short-lived. Then, for (1) to be useful, we need to replace the concentration of atomic O and H with expressions in terms of related long-lived species.

Since the O/O_3 partitioning of active-O is in equilibrium during daylight hours at 50 km, the abundance of atomic O is related to the total amount of active-O. The reaction rates for the important sources and sinks of active-O are shown in Figure 4. The active-O group is in photochemical steady state; the production of active-O (see Table 1), primarily,

(R1) $$O_2 + h\nu \rightarrow 2O$$

is balanced by the loss,

(R17) $$O + OH \rightarrow O_2 + H$$

such that the atomic O abundance is related to the abundance of the major active-H species OH (Figure 5*b*),

$$[O] = \frac{J_1[O_2]}{k_{17}[OH]} \tag{2}$$

At 50 km during daylight hours, the active-H group as a whole is short-lived (Figure 5*a*), and the cycling among the group species is rapid and is dominated by the reactions illustrated in Figure 6. The exchange between active- and inactive-H is in balance; thus, active-H is in photochemical steady state. The rates for the most important reactions are

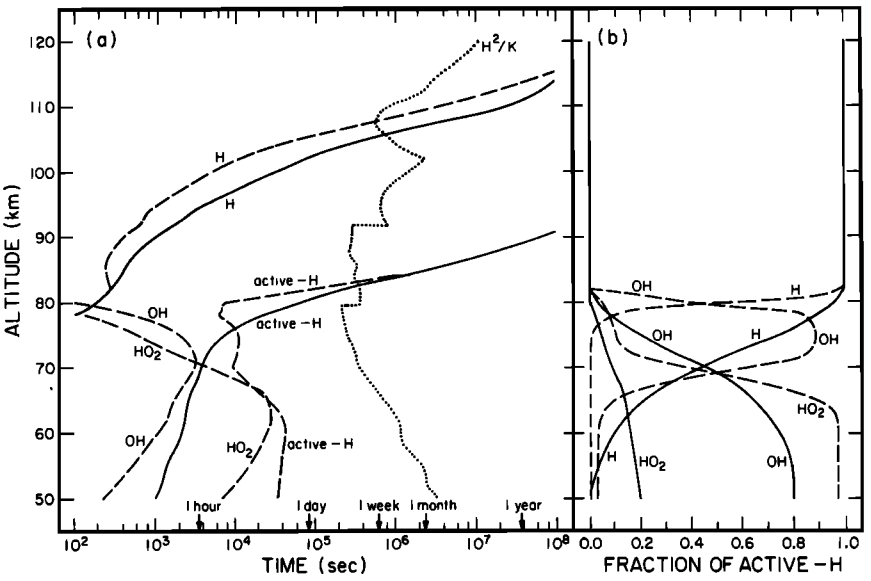

Fig. 5. Active-hydrogen species above the stratopause. (*a*) Chemical lifetimes at noon (solid lines) and midnight (dashed lines) compared with eddy diffusion time scales (H^2/K). (*b*) The relative fraction of active-hydrogen in the form of H, OH, or HO_2 at noon (solid lines) and midnight (dashed lines).

presented in Figure 7. Equating the production and loss of active-H, one finds that

$$k_{10}[O(^1D)][H_2O] = k_{23}[OH][HO_2] \quad (3)$$

The existence of $O(^1D)$ is extremely transitory, a balance between photolytic production,

(R4) $$O_3 + h\nu \rightarrow O_2 + O(^1D)$$

and loss via quenching,

(R8) $$O(^1D) + O_2 \rightarrow O + O_2$$

and

(R9) $$O(^1D) + N_2 \rightarrow O + N_2$$

so that

$$[O(^1D)] = \frac{J_4[O_3]}{k_8[O_2] + k_9[N_2]} \quad (4)$$

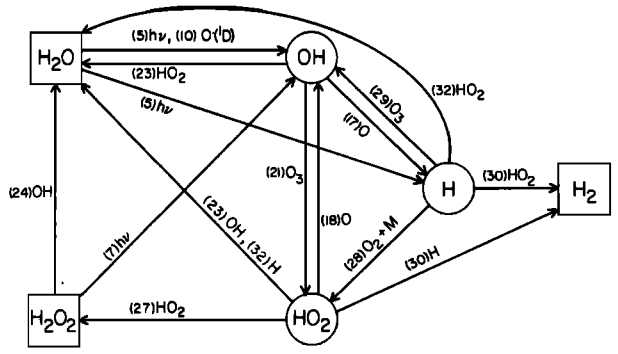

Fig. 6. Important reactions for recycling among active-hydrogen species and for conversion from active-hydrogen to inactive-hydrogen and vice versa.

The OH concentration is a balance between the reactions

(R18) $$O + HO_2 \rightarrow OH + O_2$$

and R17 with the result

$$[OH] = \frac{k_{18}[O][HO_2]}{k_{17}[O]} = \frac{k_{18}[HO_2]}{k_{17}} \quad (5)$$

Substituting (4) and (5) back into (3), one finds

$$\frac{J_4 k_{10}[H_2O][O_3]}{k_8[O_2] + k_9[N_2]} = \frac{k_{17}k_{23}[OH]^2}{k_{18}} \quad (6)$$

Substituting an expression for OH derivable from (6) back into (2), we obtain an expression containing the concentrations only of active-O species and long-lived background atmosphere species,

$$[O] = \frac{J_1[O_2](k_8[O_2] + k_9[N_2])^{1/2}k_{23}^{1/2}}{(J_4 k_{10}k_{17}k_{18}[H_2O][O_3])^{1/2}} \quad (7)$$

Upon eliminating the terms in (1) least important for daylight hours at 50 km (e.g., the nonphotolytic O_3 loss channels) and the minor terms in (7), solving for O_3 yields the result

$$[O_3]_{50} \approx \frac{J_1^{2/3}(k_9k_{23})^{1/3}(k_{14}[O_2] + k_{15}[N_2])^{2/3}[N_2]^{1/3}[O_2]^{4/3}}{(J_3 + J_4)^{2/3}(J_4k_{10}k_{17}k_{18})^{1/3}[H_2O]^{1/3}} \quad (8)$$

Thus we have an expression for O_3 in terms of long-lived atmospheric species and measurable physical parameters. The daytime variation of O_3 is now explicitly related to the collective variation in the photolytic rate constants. It is interesting to note in Figure 3 that the mesosphere is a sink for stratospheric O_3, but the upward transport of O_3 across

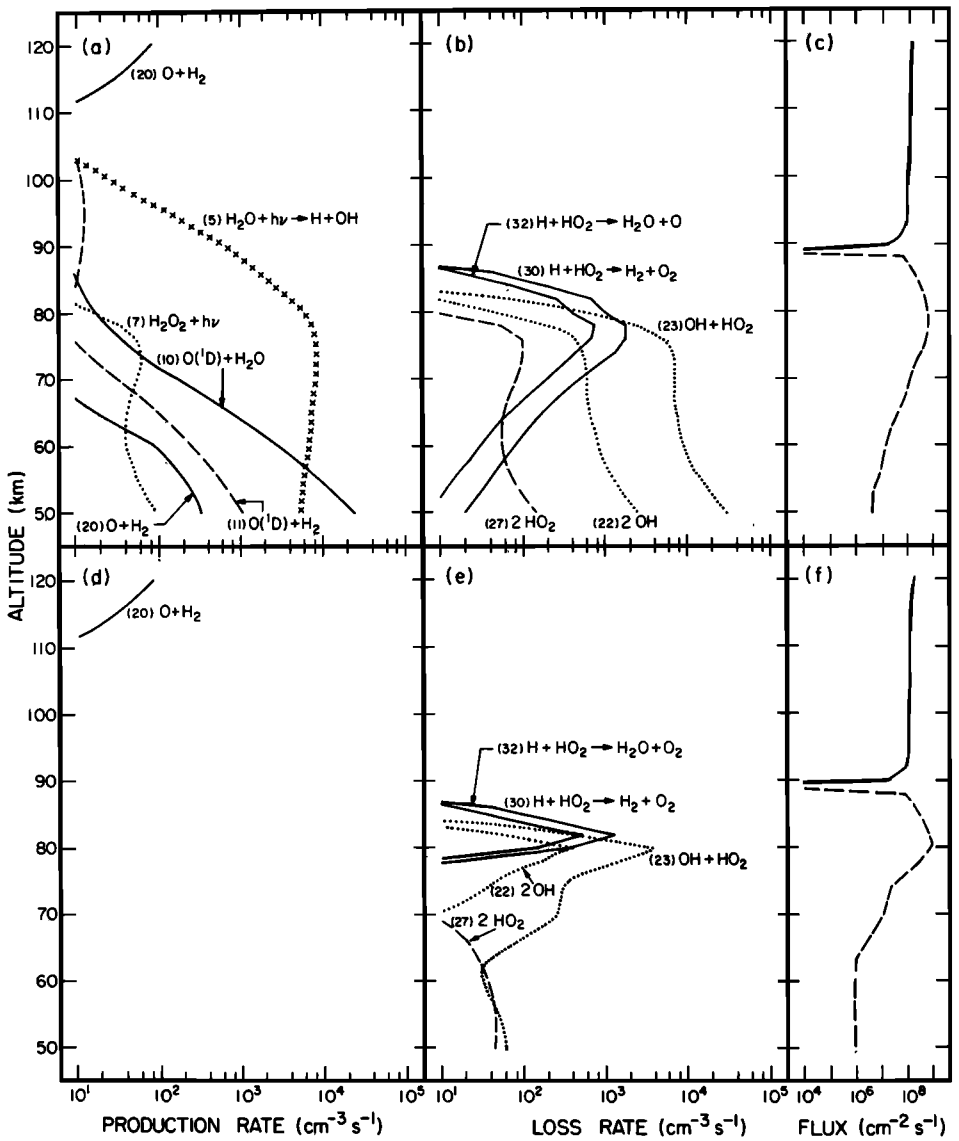

Fig. 7. Active-hydrogen chemistry. The rates of production and loss of active-H at noon, (*a*) and (*b*), respectively, and at midnight, (*d*) and (*e*). The vertical transport of active-H at (*c*) noon and at (*f*) midnight (upward flux: solid lines; downward flux: dashed lines).

the stratopause is small when compared with the magnitude of the local O_3 production and loss terms.

The interrelated active-O, active-H, and O_3 chemistries at 60 and 70 km are similar to that at 50 km. However, in the upper mesosphere, active-H results mainly from direct photolysis of H_2O,

(R5) $$H_2O + h\nu \rightarrow H + OH$$

At 60 km, both (R5) and (R10) are nearly equal in importance, so the expression for O_3 cannot be expressed as simply as (8). At 70 km, (R5) dominates, and, as a result, the daylight concentration of O_3 is then

$$[O_3]_{70} \approx \frac{J_1 k_{23}^{1/2}(k_{14}[O_2] + k_{15}[N_2])[O_2]^2}{(J_3 + J_4)(J_5 k_{17} k_{18})^{1/2}[H_2O]^{1/2}} \quad (9)$$

Whereas below 60 km O_3 is the dominant daylight form of active-O, above 60 km atomic O is the main active-O species (Figure 1*b*). So, whereas (8) actually gives the total active-O abundance at 50 km, (9) reflects both the abundance of active-O at 70 km and the minor fraction of active-O, that is, O_3.

During daylight hours at 80 km, (R29) is now competitive with (R3) and (R4) as an O_3 destruction channel:

$$[O_3] = \frac{[O][O_2](k_{14}[O_2] + k_{15}[N_2])}{J_3 + J_4 + k_{29}[H]} \quad (10)$$

Atomic H is in photochemical steady state; its density is a balance between production by (R17) and loss by

(R28) $$H + O_2 + M \rightarrow HO_2 + M$$

such that

$$[H] \approx \frac{k_{17}[O][OH]}{k_{28}[O_2][M]} \quad (11)$$

Loss of atomic H due to the reaction with O_3 (reaction (R29)) is a factor of 2 less important than (R28). Photochemical steady state for active-O results in the expression

$$(J_1 + J_2)[O_2] \approx k_{17}[O][OH] \quad (12)$$

As atomic H is the dominant active-H species at the mesopause, the result of substituting for OH in (11) using (12) shows atomic H and, therefore, active-H, being controlled by the production of active-O:

$$[H] \approx \frac{(J_1 + J_2)}{k_{28}[M]} \quad (13)$$

The active-O concentration, in turn, is related to the abundance of active-H. Since active-H is roughly in photochemical steady state and its main loss pathway is now

(R30) $$H + HO_2 \rightarrow H_2 + O_2$$

we find that

$$J_5[H_2O] = k_{30}[H][HO_2] \quad (14)$$

The production of HO_2 (reaction (R28)) is balanced by its loss rates (predominantly due to (R18)), such that HO_2 is in equilibrium with atomic H,

$$[HO_2] = \frac{k_{28}[H][O_2][M]}{k_{18}[O]} \quad (15)$$

Substituting (13) and (15) into (14),

$$[O] = \frac{(J_1 + J_2)^2 k_{30}[O_2]}{J_5 k_{18} k_{28}[H_2O][M]} \quad (16)$$

Given (13) and (16), (10) can now be rewritten to obtain the daylight O_3 concentration at 80 km,

$$[O_3]_{80} \approx \frac{(J_1 + J_2)^2 k_{30}(k_{14}[O_2] + k_{15}[N_2])[O_2]^2}{J_5 k_{18} k_{28}[H_2O][M]\left[J_3 + J_4 + \frac{k_{29}}{k_{28}}\frac{(J_1 + J_2)}{[M]}\right]} \quad (17)$$

As mentioned earlier, the mesopause is a transition region for ozone chemistry. Whereas below the mesopause, the O_3 lifetime is very long during the night, at the mesopause the nighttime lifetime becomes less than 1 hour so that it is chemically active throughout the 24-hour diurnal cycle. However, both active-O and active-H, although short-lived, are not in steady-state (loss far exceeds production), and, so a useful analytic expression for nighttime O_3 at 80 km cannot be derived.

The chemistry of ozone is most simply understandable at 90 and 100 km. The production and loss of O_3 is in balance throughout the full diurnal cycle. The lifetime of atomic O is ~1 week at 90 km and 6 months at 100 km (Figure 2). Although the time scale for conversion of atomic H to some other form of active-H is short (Figure 5), atomic H is reformed as rapidly. Since the lifetime of active-H is extremely long and the cycling within the active-H group results in atomic H being the dominant

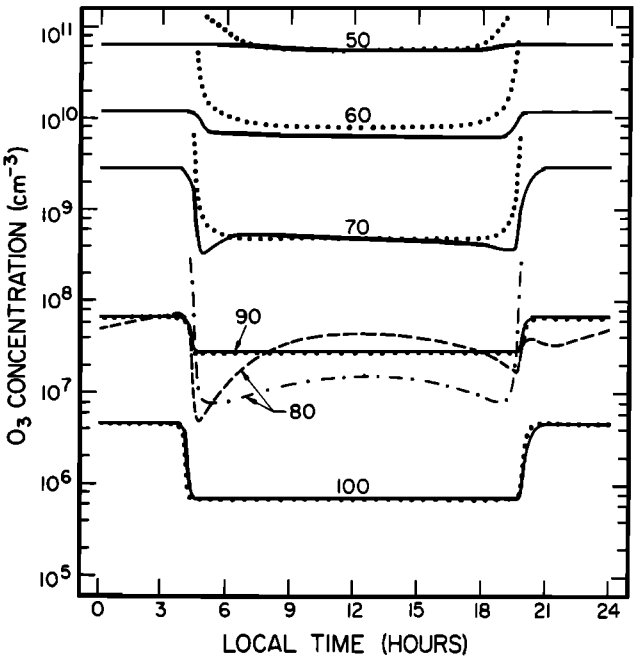

Fig. 8. The diurnal variation of ozone in the basic model of this paper: solar minimum flux, summer solstice sun at 38°N latitude, 7 ppmv of H_2O at 40 km, eddy diffusion profile of Paper I, kinetic rate constants as tabulated in Table 1, and temperature profile of Paper I increased by 20 K. Results are shown for 50, 60, 70, 80, 90, and 100 km altitudes (solid and dashed lines). Shown for the purposes of comparison are the diurnal profiles obtained with the analytical expressions of Table 2 (dotted and dashed-dot lines).

member throughout the diurnal cycle, the atomic H concentration remains constant over a 24-hour period. Therefore (1), as is, represents the diurnally varying O_3 concentration, where production terms (R13)-(R15) and the chemical loss terms (R16) and (R29) are constant and the photolytic loss terms J_3 and J_4 exist only during daylight hours.

Diurnal calculations can be performed with the simple O_3 expressions just derived and compared with the results of a detailed calculation solving the continuity equations to test the analytical formulae. Such a comparison is shown in Figure 8; the rate constants and abundances of long-lived species are the same in both calculations. The simplified calculations for nighttime are shown only above 80 km, in which altitude range there are nonsingular values for the O_3 densities. It is clear from Figure 8 that the O_3 concentrations above 80 km throughout the full diurnal period can be reproduced by the analytical expression (1) very accurately. Below 80 km, where O_3 is long-lived at night, the assumption of steady state for O_3 and active-O and/or active-H fails near sunrise and sunset, explaining the significant differences between the two calculations at those local times. The daytime O_3 densities are accurately computed in the simple calculations for most of the daylight period at 50 and 70 km. At 60 km, the analytical expression employed was simply an average of the equations for 50 and 70 km, leading to an error of 33% for most of the daylight period. Of the derivations of simple O_3 expressions presented in this paper, the one most in error is for 80 km because of the assumption that active-H is in photochemical steady state. In reality, active-H is fairly long-lived during the daylight period (Figure 5), and its production and

TABLE 2. Ozone Concentration Under Conditions of Photochemical Equilibrium

	Equations
50 km (daylight hours)	$[O_3] \approx \frac{J_1^{2/3}(k_9k_{23})^{1/3}(k_{14}[O_2] + k_{15}[N_2])^{2/3}[N_2]^{1/3}[O_2]^{4/3}}{(J_3 + J_4)^{2/3}(J_4k_{10}k_{17}k_{18})^{1/3}[H_2O]^{1/3}}$
60 km (daylight hours)*	
70 km (daylight hours)	$[O_3] \approx \frac{J_1k_{23}^{1/2}(k_{14}[O_2] + k_{15}[N_2])[O_2]^2}{(J_3 + J_4)(J_5k_{17}k_{18})^{1/2}[H_2O]^{1/2}}$
80 km (daylight hours)	$[O_3] \approx \frac{(J_1 + J_2)^2k_{30}[O_2]^2(k_{14}[O_2] + k_{15}[N_2])}{J_5k_{18}k_{28}[M][H_2O](J_3 + J_4 + \frac{k_{29}(J_1 + J_2)}{k_{28}[M]})}$
above 90 km	$[O_3] = \frac{[O][O_2](k_{13}[O] + k_{14}[O_2] + k_{15}[N_2])}{J_3 + J_4 + k_{29}[H] + k_{16}[O]}$

J_n and k_n are photolytic and kinetic rate constants, respectively, and n refers to the reaction index in Table 1.

*Expression intermediate between that for 50 km and that for 70 km.

loss terms are not in balance (Figure 7). This leads to a difference between the simple analytical and detailed computations of as much as a factor of three at noon. Figure 8 shows that the analytical expressions for O_3 reproduce the trends of the detailed computer model in general. At certain altitudes for particular local times, the values for O_3 from the simple expressions are in such good agreement with the results of the detailed computations that these expressions can be used in other types of aeronomic models where the presence of O_3 is important to the processes being considered, but a full treatment of the O_3 chemistry is awkward.

Numerical Sensitivity Analyses

The simple analytical expressions we have derived for O_3 densities are summarized in Table 2. With these equations, we can calculate the sensitivity of the O_3 distribution to changes in any of the input physical or atmospheric parameters. This also can be done numerically by performing a series of computer model calculations, which also tests the validity of these simple expressions. For this purpose, a sequence of steady state computer calculations with a diurnally averaged radiation field were executed, in each case one of the photolytic or kinetic rate constants being doubled. The changes in the model O_3 values relative to the results of the basic model of Table 1 are presented in Table 3. The diurnally averaged steady state calculation is very similar to a late afternoon steady state calculation, which in turn yields results very close to late afternoon results of a diurnal calculation since O_3 and the other key short-lived species are almost in near-instantaneous steady state during daylight hours at all altitudes.

A comparison of Table 2 and 3 reveals that almost all parameters which, when doubled, would change the O_3 concentration by more than 10% are accounted for in the simple analytical expressions at the appropriate altitudes. However, Table 3 shows O_3 to be fairly sensitive to certain reactions not appearing in Table 2 as a result of the nature of the steady state diurnally averaged calculations used to generate Table 3. On the longer time scales of these computations, species with chemical lifetimes greater than a day will be affected, which in turn influences the O_3 distribution. On the other hand, these reactions are unimportant in terms of the details of diurnal changes, the basis on which Table 2 was derived. For example, as discussed in Paper I, the atomic O thermospheric distribution is a balance between photolytic production (reactions (R1) and (R2)) and downward transport. The photolytic reaction (R6) converting H_2O to H_2 indirectly affects O_3 at 80 km and above because of its impact on the vertical distribution of long-lived, but not inert, H_2O. The photolytic reaction (R5) is the main source of active-H in the thermosphere, which in turn is important for controlling the O_3 distribution. The reaction between atomic O and O_3 (reaction (R16)) is indicated in Table 3 to be important at 50 km but has not been accounted for in the above equations. This is because R16 is less important than O + OH (reaction (R17)) as a loss mechanism for active-O in the basic model of Table 1 but is the primary loss channel if (R16) is doubled. Then the analytical expression for O_3 at 50 km during daylight hours (8) would be instead

$$[O_3]_{50} = \frac{J_1^{1/2}(k_{14}[O_2] + k_{15}[N_2])^{1/2}[O_2]}{(J_3 + J_4)^{1/2}k_{16}^{1/2}} \quad (18)$$

the importance of (R16) now being clear. The sensitivity of O_3 at 80 km to (R23) as seen in Table 3 shows that (R23) still is an important active-H loss process although Table 3 also indicates that (R30) is even more important, as was assumed in deriving the analytical expression at 80 km.

Model Calculations of Diurnal Variability

Given the validity of the simple expressions in Table 2 for representing the key processes affecting O_3, we can now use these equations to understand the detailed diurnal profiles of O_3 generated by the computer calculations. The diurnal variation of O_3 resulting from a diurnal calculation run with the Table 1 parameters is shown in Figure 8 and the analogous results for O, H, OH, and HO_2 in Figure 9. Similar calculations covering some or all of our altitude

TABLE 3. Model Ozone Variation Resulting From Input Parameter Change

Perturbation	Altitude, km					
	50	60	70	80	90	100
Doubling the rate constant						
(R1) $O_2 + h\nu \rightarrow 2O$	+58%	+55%	+71%	+82%	+21%	+9%
(R2) $O_2 + h\nu \rightarrow O + O(^1D)$	—[a]	—	+2%	+34%	+50%	+41%
(R3) $O_3 + h\nu \rightarrow O_2 + O$	−8%	−8%	−10%	−4%	−5%	−9%
(R4) $O_3 + h\nu \rightarrow O_2 + O(^1D)$	−40%	−42%	−42%	−21%	−26%	−41%
(R5) $H_2O + h\nu \rightarrow H + OH$	−2%	−9%	−24%	−41%	−19%	−4%
(R6) $H_2O + h\nu \rightarrow H_2 + O(^1D)$	—	+1%	+4%	+36%	+24%	+5%
(R7) $H_2O_2 + h\nu \rightarrow 2OH$	—	—	—	—	—	—
(R8) $O(^1D) + O_2 \rightarrow O + O_2$	+3%	+4%	+1%	+1%	+1%	—
(R9) $O(^1D) + N_2 \rightarrow O + N_2$	+9%	+8%	+2%	+2%	+1%	—
(R10) $O(^1D) + H_2O \rightarrow 2OH$	−10%	−11%	−3%	−1%	−1%	—
(R11) $O(^1D) + H_2 \rightarrow H + OH$	—	−1%	−1%	−2%	−1%	−1%
(R12) $2O + M \rightarrow O_2 + M$	—	—	—	−3%	−10%	−5%
(R13) $O + O_2 + O \rightarrow O_3 + O$						
(R14) $O + O_2 + O_2 \rightarrow O_3 + O_2$	+59%	+57%	+77%	+51%	+68%	+97%
(R15) $O + O_2 + N_2 \rightarrow O_3 + N_2$						
(R16) $O + O_3 \rightarrow 2O_2$	−23%	−9%	—	+1%	—	−5%
(R17) $O + OH \rightarrow O_2 + H$	−11%	−19%	−25%	−9%	+2%	—
(R18) $O + HO_2 \rightarrow OH + O_2$	−10%	−17%	−25%	−35%	−4%	−1%
(R19) $O + H_2O_2 \rightarrow OH + HO_2$	—	—	—	—	—	—
(R20) $O + H_2 \rightarrow OH + H$	—	—	—	—	—	—
(R21) $OH + O_3 \rightarrow HO_2 + O_2$	—	—	—	—	—	—
(R22) $2OH \rightarrow H_2O + O$	+1%	+2%	+3%	+2%	—	—
(R23) $OH + HO_2 \rightarrow H_2O + O_2$	+9%	+19%	+30%	+16%	—	—
(R24) $OH + H_2O_2 \rightarrow H_2O + HO_2$	—	—	—	—	—	—
(R25) $OH + H_2 \rightarrow H_2O + H$	—	—	—	−2%	−1%	—
(R26) $HO_2 + O_3 \rightarrow OH + 2O_2$	—	—	—	—	—	—
(R27) $2HO_2 \rightarrow H_2O_2 + O_2$	—	—	—	—	—	—
(R28) $H + O_2 + M \rightarrow HO_2 + M$	+2%	+5%	+8%	−11%	+3%	+1%
(R29) $H + O_3 \rightarrow OH + O_2$	−4%	−8%	−12%	−36%	−37%	−14%
(R30) $H + HO_2 \rightarrow H_2 + O_2$	—	—	+3%	+32%	+5%	+1%
(R31) $H + HO_2 \rightarrow 2OH$	—	—	—	−1%	—	—
(R32) $H + HO_2 \rightarrow H_2O + O$	—	—	+1%	+10%	+1%	—
(R33) $2H + M \rightarrow H_2 + M$	—	—	—	—	—	—
(R35) $CH_4 + OH \rightarrow CO + OH + 2H_2O$	—	—	—	—	—	—
(R36) $CH_4 + O \rightarrow CO + 2OH + H_2O$	—	—	—	—	—	—
(R37) $CH_4 + O(^1D) \rightarrow CO + 2OH + H_2O$	—	—	—	—	—	—
Change in solar flux from solar minimum to solar maximum[b]	—	—	—	+10%	+29%	+29%
Change in solar illumination from summer solstice to winter solstice	+11%	+10%	+33%	−13%	−33%	−20%
Reduction of H_2O boundary condition at 40 km from 7 ppm to 5 ppm	+5%	+8%	+13%	+39%	+17%	+4%
Temperature profile reduced by 20 K	+34%	+22%	+26%	+22%	+40%	+36%

Steady state computations performed with diurnally averaged solar insolation. The basic model described in the text is the point of reference.

[a]Less than ±1%.

[b]Solar minimum spectrum from *Rottman* [1981] and solar maximum spectrum from *Mount and Rottman* [1981].

range have been performed most recently by *Logan et al.* [1978], *Keneshea et al.* [1979], *Rusch and Liu* [1981], *Prather* [1981], and *Wang et al.* [1981]. The day-to-night variation and diurnal structure reported by the first four references is comparable to what is shown in Figure 8. *Logan et al.* [1978], *Keneshea et al.* [1979], and *Rusch and Liu* [1981] also display diurnal profiles for the other active-O and -H species; the results are similar to our Figure 9. The diurnal variation of OH calculated by *Herman* [1979] is also qualitatively similar to our calculations. However, not in agreement with our results and the results of the other references is the O_3 diurnal variability in the mesosphere of *Wang et al.* [1981], which is an order of magnitude larger, but not enough information is given in that paper to identify possible causes of the differences. To aid in analyzing the O_3 diurnal profiles (Figure 8) in light of the simple analytical expressions derived earlier (Table 2), we show in Figure 10 the diurnal variation of the key photolytic rate constants.

Throughout the night at 50 km, the O_3 density remains unchanged (Figure 8) because the chemical loss time scale for O_3 at night is much longer than 1 day (Figure 2) due to the disappearance of the photolytic loss term and of atomic O and H (Figure 9). The transport time scale is also too long to result in any nighttime variation in O_3. During the daytime, the lifetime of atomic O relative to recombination to form O_3 is shorter than the O_3 dissociation lifetime so that as soon as O_3 is photodissociated the atomic O formed recombines to form O_3. Therefore, the O/O_3 ratio remains relatively constant throughout the day. Moreover, active-O is destroyed almost as rapidly as it is produced so that there is little net change in the active-O abundance throughout the diurnal cycle, the photolytic source of active-O and indirect photolytic source of active-H maintaining a balance

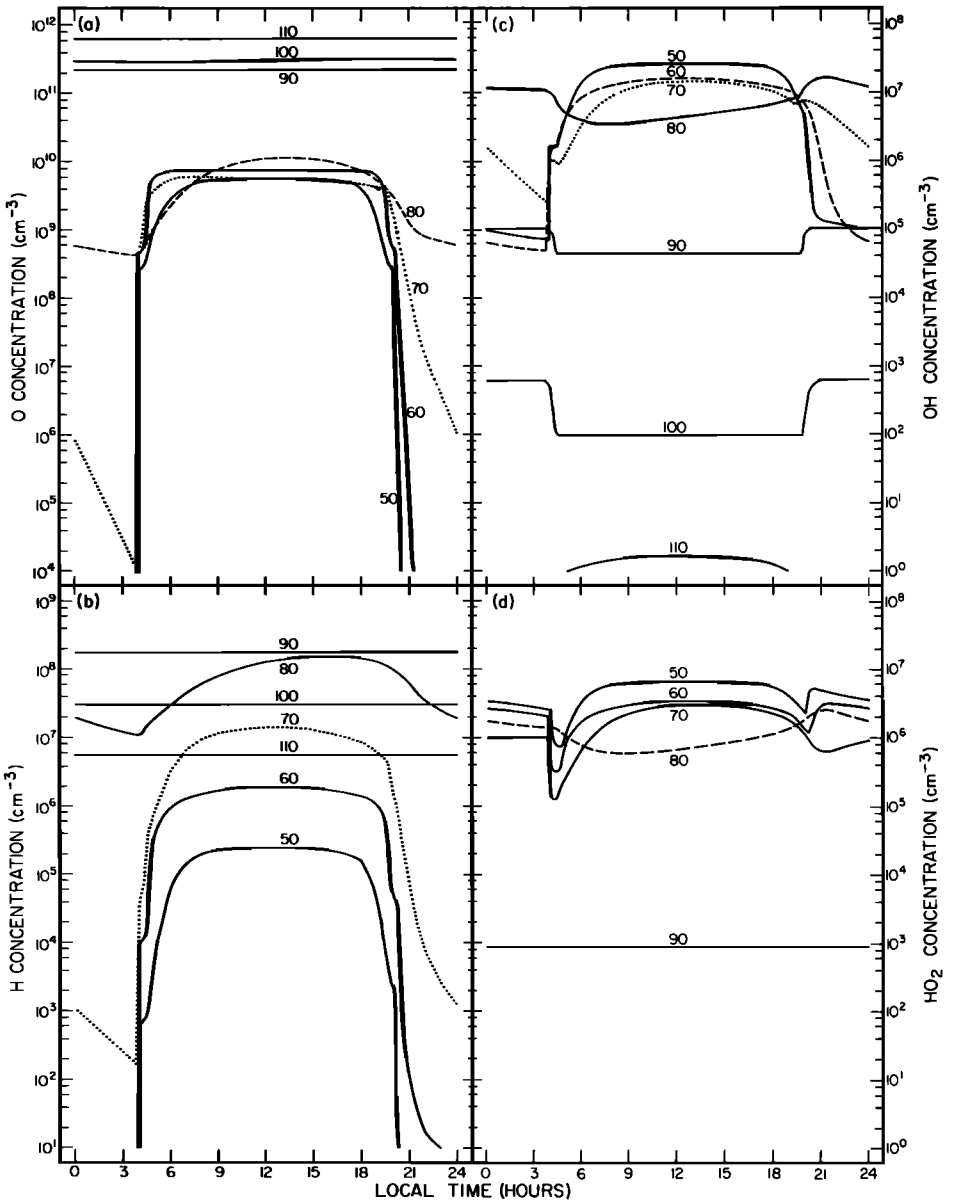

Fig. 9. The diurnal variability of (*a*) atomic O, (*b*) atomic H, (*c*) OH, and (*d*) HO_2 in the basic model for altitudes 50, 60, 70, 80, 90, 100, and 110 km.

with changing solar zenith angle. The key photolytic rate constants vary in a similar manner throughout the daylight period so that $J_1^{2/3}/(J_3 + J_4)^{2/3}J_4^{1/3}$ (see Table 2) changes very little. The day/night variation in O_3 at 50 km is very small, the difference that does occur reflecting a small decrease in the active-O abundance from night to day resulting from excess active-O loss in the morning that is offset by excess active-O production in late afternoon.

At 60 km, the relatively constant O_3 concentration at night has the same explanation as for 50 km. A moderate decrease in the O_3 density at sunrise and increase at sunset is due to the near instantaneous change in O_3 photodissociation ($J_3 + J_4$) (the atmosphere having become optically thin in the key wavelength range) without a compensating variation in active-O photolytic production. A new equilibrium between O and O_3 is established which remains in balance ($J_3 + J_4$ remaining constant) throughout the daylight hours. Also remaining in balance during the daylight period is the production and loss of active-O, driven directly or indirectly by photolysis. The near constancy of the active-O abundance is a result of the ratio $J_1/J_3^{1/2}$ remaining constant with changing solar zenith angle. The daytime near balance between active-O production and loss means that active-O does not vary much throughout the full diurnal cycle, although in fact there is a small increase in the active-O abundance from night to day. Thus, the day-to-night difference in O_3 is primarily a result of the changing atomic O/O_3 ratio.

At 70 km, the constant nighttime O_3 density and the sharp transitions at sunrise and sunset have the same explanation as at 60 km. However, at 70 km, the photolytic source of active-O increases more rapidly than the photolytic source of active-H, resulting in an early rise in the active-O abundance leveling off toward midday as a balance

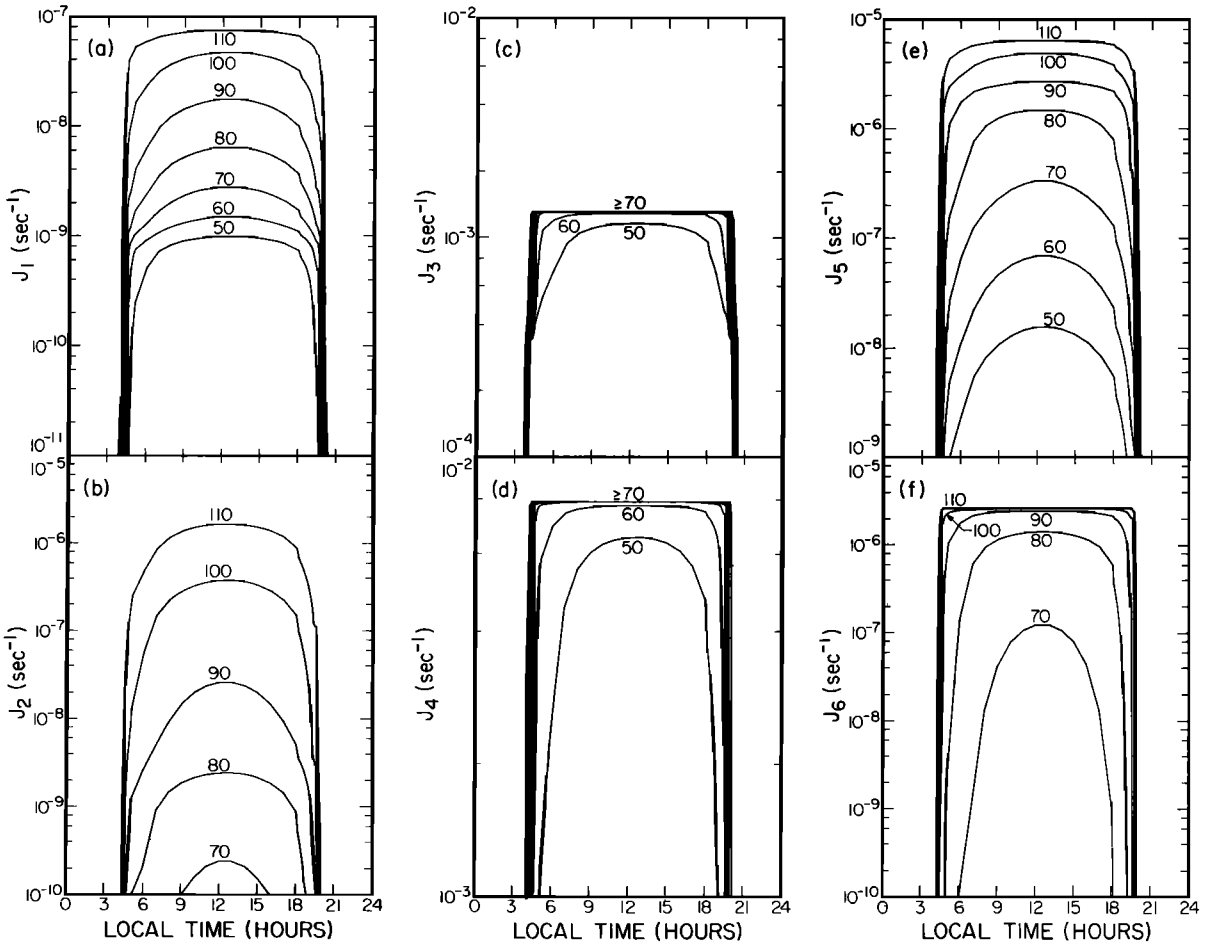

Fig. 10. The diurnal variation of the photodissociation rate constants (*a*) J_1, (*b*) J_2, (*c*) J_3, (*d*) J_4, (*e*) J_5, and (*f*) J_6 for the illumination conditions appropriate for the basic model. Results shown for 50, 60, 70, 80, 90, 100, and 110 km altitude.

with active-H catalyzed active-O loss is established, keeping the O_3 profile nearly constant throughout the remaining daylight hours. The fundamental cause of the daylight variation is the fact that the crucial wavelength range for O_2 photodissociation is optically thinner at 70 km than the wavelength range for H_2O photodissociation. Thus, at 70 km, there is an appreciable night-to-day increase in active-O, but the daytime photolytic redistribution between atomic O and O_3 results in the calculated night-to-day decrease in O_3.

The complex nature of the O_3 chemical cycle at the mesopause is reflected in a most unusual diurnal profile for O_3 at 80 km. Somewhat similar structure is seen in the calculations of *Keneshea et al.* [1979], *Prather* [1981], and *Wang et al.* [1981]. The sharp changes at sunrise and sunset are due to the instantaneous appearance and disappearance of O_3 photodissociation, J_3 and J_4. The analytical expression for O_3 at 80 km (equation (17)) shows that changes in the production of active-O with the varying sun angle are amplified relative to the changes in active-H catalytic destruction. If active-O were truly in photochemical steady state throughout the daylight period, the diurnal variation of $(J_1 + J_2)^2/J_5$ would lead to a daylight O_3 variation similar to what is shown in Figure 8. However, the morning net increase in active-O, resulting in both increasing O_3 (Figure 8) and atomic O (Figure 9), is accentuated by the reality that the production of active-O is somewhat larger than its rate of loss. By noon, production and loss of active-O are in balance. In the afternoon, production of active-O declines, and, owing to the longer lifetime of active-H, active-H is still increasing somewhat, resulting in active-O destruction exceeding its production. At sunset there is a brief increase in O_3 with the elimination of photodissociative loss, but then the abundance declines due to the continuing chemical loss of active-O. As the rate of active-O loss is proportional to the abundance of active-O, the decrease slows as active-O and active-H are depleted. Moreover, the flow of active-O from higher altitudes becomes comparable to the rate of chemical loss (Figure 4*f*). Thus, the abundance of active-O becomes relatively constant after midnight. During the nighttime period, some atomic-O recombines to form O_3 such that the percentage of active-O in the form of O_3 steadily increases. As a result, the decrease in active-O is more than offset and the O_3 abundance starts increasing near midnight.

Above 85 km, the chemical lifetimes of atomic O and H are longer than 1 day, so their abundances are constant over the diurnal cycle. Therefore, the active-O abundance and the production and chemical loss terms for O_3 are constant throughout the diurnal cycle, while the photolytic par-

titioning between atomic O and O_3 (reactions (R3) and (R4)) appears and disappears sharply at sunrise and sunset. This then produces a constant nighttime and lower constant daytime profile for O_3 in the lower thermosphere.

VERTICAL DISTRIBUTION OF O_3

Aladdin 74 Ozone Observations

One of the most detailed observational data sets covering the distribution of ozone in the mesosphere and lower thermosphere resulted from the Aladdin 74 rocket program [*Weeks et al.*, 1978]. Much of the altitude range between 50 and 110 km was monitored nearly simultaneously by more than one experimental technique. In Paper I, measurements of the major constituents of the atmosphere obtained with a mass spectrometer on one of the Aladdin 74 flights [*Trinks et al.*, 1978; *Trinks and Fricke*, 1978; H. Trinks, private communication, 1979] allowed a determination of the eddy diffusion profile above 90 km appropriate for the time of the Aladdin 74 program and gave some sense of eddy diffusion and mesospheric water content below that altitude. These data in conjunction with Millstone Hill incoherent scatter radar results (W. Oliver, private communication, 1980) also allowed a good estimate of the temperature profile in the lower thermosphere. Thus more information about general background atmosphere conditions is available for the epoch of the Aladdin 74 ozone measurements than is generally available for other O_3 data sets. For these reasons, the Aladdin 74 O_3 data seemed to present a nearly ideal case for testing in detail model results for the O_3 distribution. Preliminary work in this regard suggested that the O_3 concentration at the mesopause is reflective of certain aspects of the background atmosphere and of the validity of kinetic rate constants used in the model. These results briefly quoted in Paper I will be discussed more fully in the current paper.

Four different rocket-borne procedures for measuring high altitude ozone were flown on June 29 and 30, 1974, during rocket flights originating from Wallops Island, Virginia (38°N latitude). The chemiluminescent sondes, ultraviolet absorption and airglow photometers, and mass spectrometer had different operational altitude ranges, but the overlap of the varying altitude coverages allowed O_3 concentrations to be measured by more than one technique at most levels in the mesosphere and lower thermosphere. The intercomparisons allowed an assessment to be made of the systematic differences between the various measurement techniques.

The rocket flights that carried aloft the various instruments occurred during a late afternoon period and a period after dawn. An ozone vertical profile is shown in Figure 11, which is a composite of the Aladdin 74 results. The range of uncertainty in the value at each altitude reflects (1) the sum of the spread between the results of equally precise methods (as judged from the relative magnitudes of the published error analyses) and the error bars of the measurement being combined or (2) the errors of a lone measurement (where only one was available or where one technique was significantly more precise than the other available at the particular altitude). The O_3 values between 50 and 60 km come from the chemiluminescent sonde and UV absorption

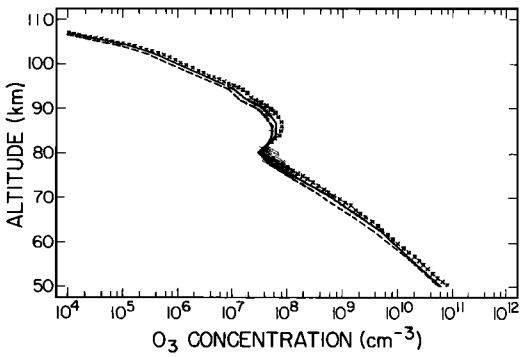

Fig. 11. The compiled Aladdin 74 rocket measurements of ozone with associated measurement errors (shaded area) and the diurnally averaged O_3 results of the basic model (solid line), the 4 P.M. LST results of a diurnal calculation (dashed line), and the diurnally averaged results of the basic model when the temperature is reduced uniformly by 20 K (crosses).

photometer post-dawn flights. The values from the chemiluminescent sonde for this altitude range taken during the late afternoon and the post-dawn periods are very similar, as is predicted by model calculations (Figure 8). The data from the UV absorption technique extend to about 83 km. These data taken during the post-dawn period should be comparable with late afternoon data, given the error bars for these results and the small daytime O_3 variation below 80 km expected from the model calculations. The airglow photometer results obtained during the late afternoon flight period contribute to the composite profile between 72 and 98 km. In the altitude range in which the UV and airglow photometer measurements overlap, the agreement is very good and supportive of the aforementioned assumption. Between 90 and 108 km, the composite O_3 distribution reflects the late afternoon mass spectrometer measurements.

Since variability during daylight hours is significant near the mesopause, the composite O_3 vertical profile shown in Figure 11 is best compared with model calculations for late afternoon (solar zenith angle χ between 43 and 53°). Because the active-O and active-H species are at, or near, photochemical steady state during daylight hours, or are very long-lived, a steady state calculation with a diurnally averaged (and therefore late afternoon) radiation field should provide results appropriate for comparison with the Aladdin 74 data much more economically than running a diurnal calculation for every test parameter change. The validity of this procedure is demonstrated in Figure 11 where the results of a diurnally averaged calculation using the basic/final atmosphere and kinetic parameters (see Table 1) are seen to be very similar to results for 1600 LST (χ = 47°) from an explicit diurnal calculation (from which the results shown in earlier sections are derived). The good agreement between our model results and the observed O_3 profile in the 50- to 95-km altitude range only results after a variety of parameters are modified.

Derivation of Basic Model Parameters

When we initiated this investigation, the most currently available rate constants were those summarized in *Hudson and Reed* [1979]. In the interim, laboratory investigations

resulted in revision to some of these values (summarized most recently in *DeMore et al.* [1982]). With these new rate constant values, model calculations match O_3 observations much better. In this section, we will show the importance of some of these modifications in rate constants and illustrate how a careful comparison between model calculations and observations can indicate potential changes in the accepted values for key rate constants and climatological variables.

The first test comparison is between the Aladdin 74 data and model computations utilizing the *Hudson and Reed* [1979] rate constants, a diurnally averaged radiation field, the density-temperature profile for the background atmosphere discussed in Paper I, and the eddy diffusion coefficients above 90 km whose derivation is also discussed in Paper I. The eddy diffusion profile $K(z)$ below 90 km (see profile 1 in Figure 12*a*) is that recommended by *Hudson* [1977], which is basically double the magnitude of the eddy diffusion profile suggested by *Hunten* [1975] and results in good agreement between models and observations of the vertical profiles of stratospheric tracer species. The lower boundary condition at 40 km for H_2O in this calculation is 5 ppmv, the value suggested by the radio measurements of mesospheric water obtained by *Waters et al.* [1980]. A comparison between the model results thus obtained and the Aladdin 74 composite profile is shown in Figure 12*b*. The theoretical and observational results are in good agreement, except between 75 and 90 km and above 95 km. At the mesopause the discrepancy is as large as a factor of 15 peaking around 83 km. Although wavelike deviations from a mean value can be produced by upward-propagating gravity waves, *Frederick* [1979] using gravity wave parameters derived from observations shows that this could only produce a variation of less than 10% at 80 km and a factor of 2 at 90 km. This result taken together with the fact that a local minimum in the observed O_3 profile near 80 km and a secondary maximum near 90 km also appear in the model calculations suggests that the structure near the mesopause is a result of phenomena already included in the model but that the sources of the differences in the magnitude of the O_3 secondary maximum lie somewhere in the values for the input parameters.

Poorly known, but potentially highly variable, are the values of the climatological parameters that affect the model calculations. Least well constrained by observational data is the magnitude of vertical transport (i.e., eddy diffusion) for the altitude range from the stratopause to 90 km. Therefore, we first consider what improvement in the model fit to observation could result from modifying the eddy diffusion values chosen initially. Above 58 km, daytime O_3 is in equilibrium with the larger reservoir of atomic O. From 85 km down to 80 km, the lifetime of active-O ($\approx$ atomic O) rapidly decreases from $\sim$1 day to $\sim$1 hour (Figure 2). However, as seen in Figure 4, the downward flow of active-oxygen can contribute to the abundance of active-O at 80 km since the magnitude of the gradient of the flux is of the same order of magnitude as local chemical production and loss processes. The abundance of H_2O at 80 km, a parameter to which mesopause O_3 is sensitive, is also affected by the magnitude of vertical motion at and above the mesopause. We judged that adjusting the eddy diffusion profile between 80 and 90 km to introduce a stagnant layer would

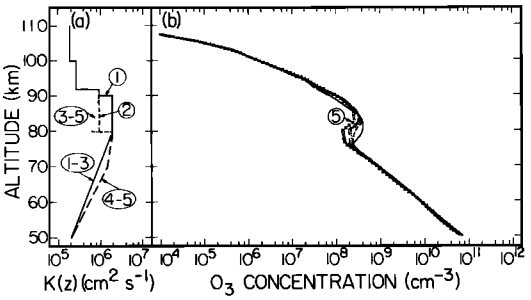

Fig. 12. (*a*) Trial eddy diffusion profiles and (*b*) consequent model O_3 results. Associated profiles in Figure 12*a* and 12*b* are indicated by the same symbol. The 40 km boundary condition for H_2O is 5 ppmv for profiles 1-4 and is 7 ppmv for 5. All O_3 profiles are derived from computations using diurnally averaged atmospheric transmission, the temperature profile of Paper I and the standard rate constants (i.e., without the adjustments suggested in this paper). Shaded area is the compiled Aladdin 74 measurement (see caption for Figure 11).

reduce the downward flux of atomic O and would retard the flow of H_2O through the mesopause, resulting in an increase in the abundance of H_2O at 80 km. The consequence of these two effects is to reduce atomic O and, in turn, O_3 concentrations at the mesopause. Trial $K(z)$ profiles (2 and 3) are shown in Figure 12*a* and the resulting O_3 distributions in Figure 12*b*. Some reduction in the model O_3 values at the secondary maximum results; a comparison of the O_3 values corresponding to trial $K(z)$ profiles 2 and 3 shows that further modification of $K(z)$ between 80 and 90 km would not result in significant further improvement. Since the abundance of H_2O at the mesopause is also strongly controlled by the rate of upward transport from the stratopause, we investigated what modification of the $K(z)$ profile between 50 and 80 km could reduce 80 km O_3 further. $K(z)$ profile number 4 (Figure 12*a*) maximizes the amount of H_2O at 80 km and does result in a small decrease in O_3.

The adjustments to the adopted eddy diffusion profile between 50 and 90 km do affect the O_3 profile even though O_3 may be short-lived. Thus, easily observable O_3 can be used as a tracer of transport in the upper atmosphere. However, the discrepancy between Aladdin 74 observations and model results remains significant.

Also poorly known is the magnitude and variability of H_2O at the mesopause. As seen in Table 2, the relative sensitivity of the O_3 concentration to the local H_2O abundance is a maximum at 80 km, and, thus, a change in the adopted 40 km boundary condition for H_2O would result in a change in the O_3 concentration largest at 80 km (Table 3) leaving the O_3 values little changed at the other altitudes where there is a good match between observations and model results. When the lower boundary condition for H_2O is increased to 7 ppmv, a value that is still consistent with the *Waters et al.* [1980] measurements and in agreement with an extrapolation of the stratospheric results of *Farmer et al.* [1980], the resulting O_3 profile (5 in Figure 12*b*) shows the expected reduction at 80 km. The new H_2O profile (Figure 5*b* in Paper I) is consistent with the unpublished 90 km Aladdin 74 mass spectrometer H_2O measurement (H. Trinks, private communication, 1979) and the recently published observational results of *Deguchi and*

Muhleman [1982] and, in the lower mesosphere, with the conclusions of *Bevilacqua et al.* [1983] and the preliminary results from the NIMBUS 7 SAMS instrument [*WMO*, 1981]. Our profile is somewhat higher than the preliminary data from the SAMS instrument for the 75-85 km altitude range [*Drummond and Mutlow*, 1981] and the upper mesospheric results of *Bevilacqua et al.* [1983] (further discussion of this is postponed to a later section). The range of values for the water vapor mixing ratio in the lower thermosphere derived from meteoritic ion observations [*Solomon et al.*, 1983] includes the H_2O values resulting from the new model calculation. Very recently, the J. E. Frederick and A. R. Douglass (private communication, 1982) analysis of stratospheric water vapor observations and the oxidation of CH_4 to H_2O finds that 7 ppmv of H_2O at the stratopause is consistent with the largest group of stratospheric measurements.

The foregoing discussion is a derivation of the $K(z)$ profile between 50 and 90 km and the 40 km H_2O boundary condition that were presented in Paper I without extensive explanation. After the changes in eddy diffusion and mesospheric H_2O distribution are made, the model values for O_3 at the mesopause are now a factor of 10 too large, a reduction of 33% from the initial calculation. At this point it seems necessary to consider what errors in the model results can be due to inaccuracies in the kinetic rate constants adopted, some of which are (or were) relatively poorly constrained by laboratory measurements. Studying the impact of the different parameters on the whole O_3 profile above the stratopause allows the best assessment of which parameters may need to be modified since, in some cases, different altitude ranges may constrain the same rate constant in opposite senses, thus allowing little room for adjustment. Such is the case for the rate constants $O + O_2 + (O_2, N_2)(k_{14-15})$; when the values are reduced to lower O_3 at 80 km, the result is too little O_3 at 60 km, suggesting that these laboratory measurements are not adjustable in light of this observational data set. Thus the rate constants listed in Table 1 for k_{14} and k_{15} are the nominal values of *Klais et al.* [1980]. (In Paper I, our preliminary analysis only concerned the sensitivity of mesopause O_3 to parameter values, thus leading us to suggest reducing k_{14} and k_{15}.)

The analysis of O_3 chemistry presented earlier in this paper and summarized in Table 2 shows that, particularly at 80 km, the O_3 concentration is especially sensitive to the values of k_{28} and k_{30} which, if increased and decreased, respectively, can cause a significant decrease in model values. Furthermore, O_3 is relatively more sensitive to k_{18} at 80 km than at any other altitude. When the values for k_{18} and k_{28} are modified within the latitude allowed by the measurement uncertainties quoted in *Hudson and Reed* [1979] and the value for k_{30} reduced in concert with the error bar for the *Hack et al.* [1978, 1979] measurement (modifications reported in Paper I), the O_3 density at the mesopause is decreased by about a factor of 5. Since the publication of Paper I, refinements of the laboratory measurements of k_{18} and k_{30} have occurred. At the low temperature of the mesopause (~170-180 K), the modified rate constant for the reaction $O + HO_2$ (reaction (R18)) reported in Paper I was a factor of 2 larger than the value derived from the recommendation of *Hudson and Reed* [1979], but *Keyser* [1982] has published a new laboratory measurement of k_{18} that, at 170 K, is even 40% larger than our value (8-83% larger given the reported uncertainties). Another recent measurement (room temperature) of k_{18} [*Sridharan et al.*, 1982] is 10% lower than the *Keyser* [1982] result and also in agreement with our conclusion that $O + HO_2$ has to occur faster than earlier laboratory measurements had indicated. If the *Keyser* [1982] value is used, O_3 is decreased too much, so we adopt a value at the lower limit of his experimental uncertainties, but it is larger than the earlier data evaluation recommendations. *Sridharan et al.* [1982] also report a new value for $k_{30} + k_{31} + k_{32}$ and a relative branching ratio for each of the individual reactions. They find that $k_{30}/(k_{30} + k_{31} + k_{32})$ is ~9%, similar to the value of 13% adopted in Paper I, which was half of that reported by *Hack et al.* [1978]. These newest measurements for k_{30-32} have been adopted for the current work and are listed in Table 1. Table 2 shows that enhancing k_{29} reduces O_3 at and above the mesopause, allowing a better match to the local minimum at 80 km and the secondary maximum at 85 km. Thus we use a value (see Table 1) that is the upper limits of the uncertainties of *DeMore et al.* [1982].

Below 70 km, model O_3 is sensitive to k_{23} which we increase slightly to improve the match between model and observations and to k_{17} which is decreased. The value for k_{23} in Table 1 is 20% higher than the zero pressure room temperature value of *DeMore et al.* [1982]. Very recently, *Kaufman et al.* [1982] reported a positive activation energy (~436 K) for this reaction that would result in faster reactions at mesospheric temperatures. The value for k_{17} is decreased within the limits allowed by *WMO* [1981] and is ~40% lower than the new lower limit suggested in *DeMore et al.* [1982].

The O_3 model results below 60 km in Figure 12*b* are at the lower end of the uncertainty range of the observations. Several processes affect the O_3 profile only in this altitude range and can be adjusted to increase the model O_3 results (see Table 2). Thus, the values in Table 1 for k_8 and k_9 are the maximum values allowed by the uncertainties in the laboratory results [*DeMore et al.*, 1982]. Similarly, k_{10} is reduced to the maximum extent [*DeMore et al.*, 1982].

The model O_3 profile resulting from making all of these adjustments in the kinetic rate constants is shown in Figure 11 (profile demarcated with crosses). The rate constants of less important reactions have been updated in accord with *DeMore et al.* [1982]. The discrepancy at the secondary maximum is significantly reduced. Although the largest changes allowed by the measurement uncertainties are implemented, the model secondary maximum is still higher than the observed value. One major model parameter not yet considered is the temperature profile, adjustment of which could allow the model results to better reproduce the observations. Since so many of the reactions in Table 1 are temperature-dependent, the ozone abundances at all altitudes are sensitive to some extent to the local value of the atmospheric temperature. The variability of O_3 in the mesosphere and lower thermosphere resulting from changes in the temperature field is a key element in the studies of *Frederick* [1979, 1981*a*, *b*]. Gravity waves can result in oscillating temperature profiles [*Frederick*, 1979]; such could have been the case at the time of the Aladdin 74 observations. Variations in temperature by as much as 25

K have been observed in a short time span in the altitude range 65-85 km (by rocket measurements also originating from Wallops Island, Virginia) [*Schmidlin*, 1976]. These temperature profiles distinctly showed a wavelike structure. Wavelike vertical temperature profiles in the mesosphere along with short-term fluctuations at a given altitude can be clearly observed by ground-based lidar soundings [*Chanin and Hauchecorne*, 1981; *Hauchecorne and Chanin*, 1982, 1983]. Differences between the temperature measurements and standard atmospheric models can be as large as 20 K.

Systematically increasing the temperature profile used in Paper I by 20 K results in an O_3 distribution that is shown in Figure 11. (Actually the temperature profile of Paper I is somewhat higher than a temperature profile derived in the appendix of that paper by a hydrostatic calculation utilizing the Aladdin 74 mass spectrometer data. However, systematic error may have been introduced into that calculation due to its limited nature, as evidenced by the resulting extreme temperature gradients, leading us to adopt more standard profiles.) Whereas the secondary maximum is now reproduced extremely well by the model calculations, the results below 70 km only marginally agree with the observations. But as seen in the lidar temperature measurements, deviations from a more "normal" temperature sometimes may only occur in a narrow altitude range at any particular point in time. Thus the temperature modification adopted for the calculations may only have occurred at the mesopause at the time of the O_3 measurements, and the standard temperature profile may be a more accurate representation of conditions in the lower mesosphere at that time. However, for the sake of simplicity, the standard atmosphere temperature profile (see Paper I) increased by 20 K is adopted for the basic model of this paper. This is implemented only for the purposes of comparison with the Aladdin 74 observations and other temperature profiles will be utilized in computations focussed on measurements at other epochs.

By this sequence of model/observation intercomparisons, we arrive at a basic model, the results from which were already used in earlier sections in which the important reactions of relevance to the O_3 chemistry were discussed. A good fit to the O_3 observations from 50 km all the way up to 95 km, spanning several different regimes of O_3 chemical cycles, only results when the kinetic rate constants, H_2O abundance, eddy diffusion coefficients, and background temperature are modified from the initial assumptions, but in each case the changes are within the limits of current uncertainties. Some of the suggestions for changes presented in Paper I subsequently have been proven to be correct. The changes we have suggested for different parameters clearly are correlated. Better determinations of any of these parameters will affect our estimates for the others, doubtlessly resulting in future revision. This then is our basic model (the climatological parameters being most appropriate for the Aladdin 74 period): the kinetic rate constants reported in Table 1, the H_2O vapor abundance and eddy diffusion coefficients previously presented in Paper I, and the background temperature profile discussed in Paper I uniformly increased by 20 K. The diurnally averaged O_3 results and the late afternoon profile of a diurnal run (the time of day for the key Aladdin 74 measurements) are shown to be similar in Figure 11, confirming that the diurnally averaged tests used to derive the basic model are appropriate when compared with observations taken at that specific time.

One group of parameters which we did not attempt to adjust to bring about better model/observation agreement is the set of photodissociation rate constants. We feel that in general these are much better known than the difficult-to-measure free radical rate constants. The model calculations shown in this paper utilize the parameterization for the O_2 Schumann-Runge bands described in Allen and Frederick (1982). After the bulk of our computations were performed, *Frederick and Mentall* [1982], *Herman and Mentall* [1982], and *Froidevaux and Yung* [1982] proposed that the values of the O_2 Herzberg continuum cross section were smaller than the values previously used in atmospheric opacity and photodissociation calculations (for example, as in *Allen and Frederick* [1982]). However, when the appropriate adjustments are made to our calculations, the resulting model O_3 values are reduced at most by 13% at 50 km and systematically less so with increasing altitude, similar to what *Ko and Sze* [1983] and *Solomon et al.* [1983] found upon including the reduced cross-section values. Such a small difference is within the uncertainties of the absolute cross-section values of the key photolytic processes. Another potential error in the model calculations related to inaccuracies in the photodissociation computations has been proposed by *Cicerone and McCrumb* [1980]. These authors suggest that a combination of quantum and optical depth effects may result in an enhanced dissociation rate for isotopically heavy O_2 ($^{18}O^{16}O$) relative to the most abundant form ($^{16}O^{16}O$) such that the current odd-oxygen production rate might be underestimated by as much as 10% in the mesosphere. A lack of detailed quantitative spectroscopic data for heavy O_2 prevents a good assessment of this possibility.

Very recently new laboratory measurements of the rate constants for $O + O_2 + M$ were reported by *Lin and Leu* [1982]. When used in our model computations (still assuming that $k_{13} = k_{14}$), the new model values for O_3 are down by 4% at 50 km relative to the basic model values, higher at 80 km by 11%, higher at 90 km by 21%, but little different at higher altitudes. This affects the simulation of the Aladdin 74 profile a little, but more importantly cannot help bring the model results above 95 km into better agreement with the observations (see Figure 11). Instead of the previously adopted assumption that atomic O and O_2 are equally efficient third-bodies in the recombination process, M. T. Leu (private communication, 1982) suggested that atomic-O may behave in a manner intermediate between He and Ar, whose third-body efficiencies had been measured [*Lin and Leu*, 1982] and also that the M = O rate constant should be doubled to reflect the symmetry in the reaction. As atomic-O becomes more abundant than O_2 above the homopause, such rate constant modifications would impact on the calculated O_3 profile in this high altitude range. When the computations are adjusted in accordance with Leu's suggestions ($k_{13} = 5.8 \times 10^{-35}\ e^{535/T}\ cm^6\ s^{-1}$), the new O_3 values are actually less than before since atoms are much less efficient third-body intermediaries than O_2 in the case of this reaction and thus the new k_{13} is smaller than that previously used. The O_3 observations at lower altitudes do not allow other key rate constants (see

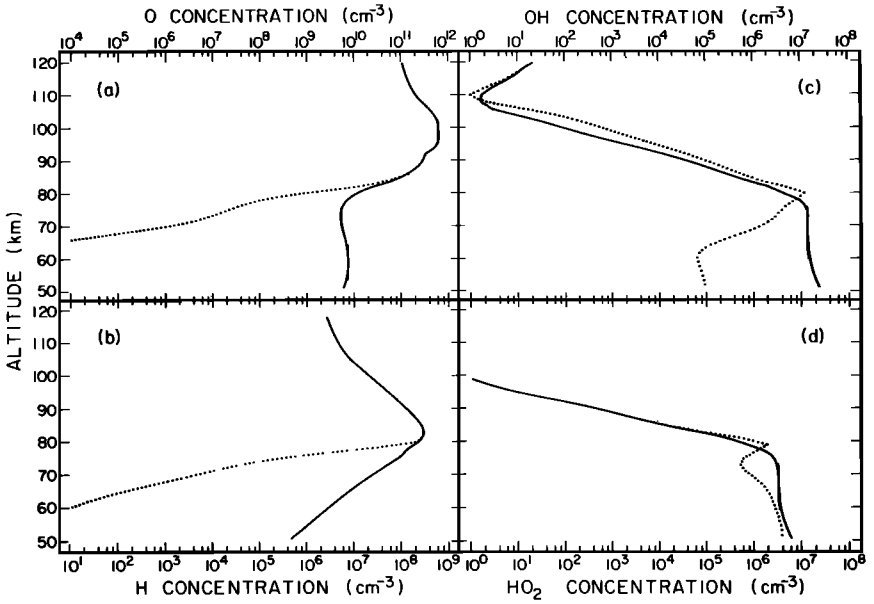

Fig. 13. Noon (solid lines) and midnight (dotted lines) altitude profiles from the basic model for (*a*) atomic-O, (*b*) atomic-H, (*c*) OH, and (*d*) HO_2.

Table 2) to be varied sufficiently to bring the model results into better agreement with the observed O_3 profile above 95 km. The important climatological parameters for the lower thermosphere at the time of the Aladdin 74 flights are also well constrained. We are currently evaluating a number of processes heretofore not considered in this context which could resolve this discrepancy.

Calculations of Atomic Oxygen

During daylight hours above 58 km, ozone is a tracer reflective of the larger amount of atomic oxygen present. If one has the correct chemical model for O/H species in the upper atmosphere, the atomic O profile must be calculated correctly for a proper O_3 profile to result. In Paper I, a model atomic O profile matching the Aladdin 74 measurements above 90 km resulted upon adjustment of the eddy diffusion profile above 90 km. The kinetic rate constants used in that study are only slightly different from what are used herein, so the atomic O profile above 90 km calculated with the basic model of this paper (see Figure 13*a*) is almost exactly that in Paper I. Many other measurements of atomic O in the lower thermosphere have been acquired, most of which are included in the compilation of *Offermann et al.* [1981]. There are very significant differences between the observed atomic profiles reported therein, and it is unclear whether the variation results from the variety of measurement techniques or from different atmospheric phenomena at different latitudes or, more generally, the temporal variation of atmospheric behavior anywhere.

A more useful test of the model of this paper can be made by using observations of atomic-O at or below the mesopause, in which altitude range atomic-O is much less sensitive to variability in eddy diffusion. Of the available measurements, two most directly comparable with the detailed calculations performed for this paper are those derived from mid-latitude summer rocket flights at solar minimum reported by *Thomas and Young* [1981] and *Baker et al.* [1982]. The observed values for atomic-O at 80 km are 3.5×10^8 cm^{-3} (midnight [*Thomas and Young*, 1981]) and $\sim 10^{10}$ cm^{-3} ($\chi = 77°$ [*Baker et al.*, 1982]), both in good agreement with our diurnal computations shown in Figures 9 and 13*a*. *Thomas and Young* [1981] also observed an atomic-O peak in the lower thermosphere very similar to the calculations in Paper I and the current work. Atomic-O profiles below the mesopause were measured by *Dickinson et al.* [1980]. Although the circumstances of these observations are not reproduced by our model runs, there is good qualitative agreement between our results displayed in Figure 13*a* and the observed profiles: (1) The daytime measurements show a steady decrease from the lower thermospheric peak down to 80 km below which the atomic-O density is relatively constant with altitude down to 60 km, holding at a value $\sim 10^{10}$ cm^{-3}; (2) nighttime atomic-O decreases rapidly and steadily from the lower thermospheric peak, dropping below measurement sensitivity ($\sim 10^9$ cm^{-3}) near 80 km.

Model Results for Hydrogen Species in the Upper Atmosphere

The model calculations of O_3 are very sensitive to the local concentrations of active-H species, which catalyze the recycling of active-O back to O_2. The sensitivity of the calculated O_3 profile to the changes in the H_2O abundance discussed earlier results from H_2O being the main source of active-H. Many of the rate constants we have adjusted to improve the O_3 model/observation comparison are important in that they affect the cycling among the active-H species and the rate of conversion of active-H to inactive forms.

Consequently, the calculated profiles of the various hydrogen species (Figures 13 and 14) also need to be consistent with observations to verify the validity of the model description of O_3 chemistry. As discussed earlier in this

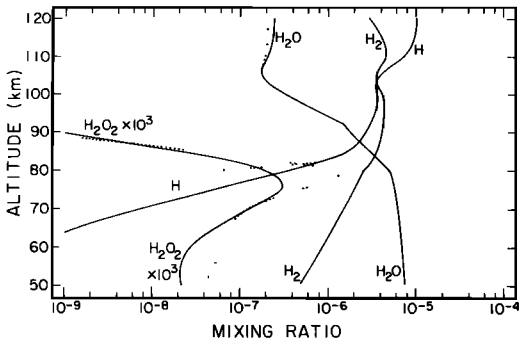

Fig. 14. The upward transport of elemental hydrogen from the stratopause to the lower thermosphere: the mixing ratios at noon (solid lines) and midnight (dotted lines) for atomic-H and the inactive-H species, H_2, H_2O, and H_2O_2, the latter scaled upward by a factor of 10^3.

paper, the adopted 40 km boundary condition for H_2O and the resulting model profile for H_2O above the stratopause are in accord with a variety of observations of H_2O in the mesosphere and lower thermosphere. Above the mesopause, inactive-H is predominantly H_2 (see Figure 14). As most of the H_2 in the lower thermosphere is derived ultimately from the H_2O flowing up through the mesosphere, the H_2 concentration profile reflects the mesospheric H_2O abundance, photodissociation rates (solar conditions, etc.), and upward transport velocities. The springtime solar minimum equatorial measurements of H_2, using an ultraviolet stellar occultation technique [*Atreya et al.*, 1976], yielded values ranging from 1×10^8 cm^{-3} (±15%) at 95 km to 1×10^7 cm^{-3} (±5-8%) at 108 km. Our model values of 9.5×10^7 cm^{-3} (95 km) and 5×10^6 cm^{-3} (108 km) are in reasonable agreement with the observational results, the differences possibly resulting from a variety of factors, including variability of vertical motion.

Unfortunately, the dominant active-H species in the daytime in the mesosphere below 70 km — OH — has only been directly measured once [*Anderson*, 1971]. The OH concentration profile calculated by the current basic model (Figure 13*c*) is very similar to what is shown in Paper I (Figure 5*a*), wherein the observational values are well fit by the model results. Above 70 km during the day and above 80 km throughout the diurnal period, atomic-H is the dominant form of active-H (cf. Figures 13*b*-13*d*). The high latitude autumn solar maximum atomic-H measurements of *Evans and Llewellyn* [1973] are an order of magnitude smaller than lower thermosphere model results (including our own run with a "solar maximum" spectrum), leading these authors to suggest a very dry mesosphere. They also measured at the same time O_3 (in fact, the atomic H results are dependent on the O_3 observations) and found more than our models generate, but consistent with O_3 chemistry as we understand it. On the other hand, the mid-latitude winter solar maximum airglow observations of *Anderson et al.* [1980] are consistent with atomic-H profiles larger than the *Evans and Llewellyn* [1973] result, but still somewhat lower than results from our model computed with solar illumination appropriate for the epoch of the *Anderson et al.* [1980] rocket flight. The uncertainties of their observational analysis do not clearly exclude our higher values for atomic-H. Recently, *Kita and Sharp* [1982] report a direct measurement of the atomic-H distribution obtained in a winter mid-latitude rocket flight (χ = 102°) when the sun was shifting to solar minimum behavior: [H] ~5×10^6 cm^{-3} at 75 km, ~5×10^7 cm−3 at 80 km, a peak of $1.4 \pm 0.8 \times 10^8$ cm^{-3} at 85 km, and $\lesssim 10^8$ cm^{-3} at 90 km. The results for atomic H from our calculation using a diurnally averaged solar minimum winter sun are 10^7, 5×10^7, 2×10^8, and 1.5×10^8 cm^{-3}, respectively, in reasonably good agreement with *Kita and Sharp* [1982]. Although a diurnal computation specific for the circumstances of the *Kita and Sharp* [1982] observations is necessary for performing a detailed comparison between model and measurements, from Figure 9, one can infer the general pattern of atomic-H diurnal variation, which when accounted for would result in values in the mesosphere at the local time of the *Kita and Sharp* [1982] measurement lower than those of a diurnally averaged sun (late afternoon) calculation. Interestingly, as shown in eqn. (13), the concentration of atomic-H in the upper mesosphere during daylight hours is relatively insensitive to the local H_2O abundance. This is seen in the results of two diurnally averaged calculations with the basic model wherein the 40 km boundary condition for H_2O in one case is 7 ppmv and in the other case 5 ppmv; the atomic-H concentrations differ by less than 5% between 65 and 80 km.

One further check on the hydrogen budget of the model concerns the upward flux of elemental hydrogen. As summarized most recently by *Hunten and Donahue* [1976], the amount of elemental hydrogen escaping from the terrestrial atmosphere (~2-3 × 10^8 atoms cm^{-2} s^{-1}) must be supplied from the lower atmosphere. Elemental hydrogen is transported upward through the stratopause in the form of H_2O, converted to H_2 near the mesopause, and then further transformed into atomic-H in the lower thermosphere (see Figure 14 and *Liu and Donahue* [1974*a*, *b*]). With our boundary conditions at 130 km for atomic H and H_2 being the maximum diffusion velocity [*Banks and Kockarts*, 1973, p. 43], the upward flow of elemental hydrogen is conserved from level to level in the model calculation and is 3.3×10^8 H atoms cm^{-2} s^{-1}. The general agreement between our value and the approximate value for the earth is a rough verification of the model mesosphere hydrogen content.

Thus, the adjustments to the model parameters (the 7 ppmv 40 km boundary condition for H_2O, the modified kinetic rate constants) that help bring the calculated O_3 profile into better agreement with the Aladden 74 results can be roughly checked with a variety of other relevant

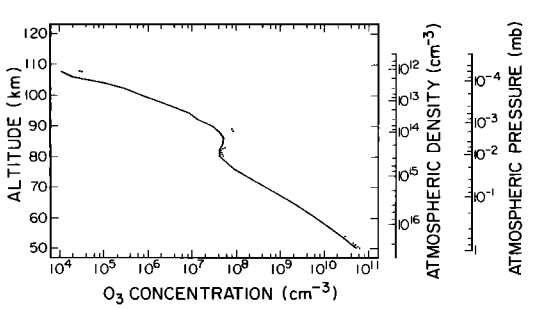

Fig. 15. The vertical distribution of O_3 at noon (solid line) and midnight (dotted line) resulting from the basic model.

observations. However, the comparisons between observations and model results, showing points of agreement and some disagreements, are only partly relevant because of the high probability of the H_2O content of the atmosphere varying with time. The H_2O concentration at the stratopause and consequently the mesosphere H_2O and active-H profiles may have been different at the time of the Aladdin 74 rocket flights (mid-latitude solar minimum 1974 summer period) considering that the observations we have examined were at different latitudes, seasons, and/or phases of the solar cycle.

O_3 *Secondary Maximum*

Shown in Figure 15 are the vertical profiles for O_3 at noon and midnight generated by a full diurnal calculation with the basic model. While both profiles show an enhancement between 80 and 90 km relative to the 80 km value, the secondary maximum is more prominent at night, there being an overall nighttime increase in O_3 above 60 km, but the contrast is also greater since the concentration of O_3 at the 80 km local minimum is coincidentally similar in magnitude at noon and midnight. The temporal variation of the secondary maximum can be roughly traced in the diurnal variation of O_3 displayed in Figure 8.

A secondary maximum in the ozone distribution at the mesopause was first inferred from high altitude observations of "excess" O_2 ($^1\Delta_g$) airglow emissions [*Evans et al.*, 1968; *Evans and Llewellyn*, 1970], resulting from O_3 photolysis. From the *Evans et al.* [1968] flight (mid-latitude, late afternoon, fall sun at solar minimum), a peak O_3 density of $\sim 10^8$ cm^{-3} at ~83 km can be derived. Using high latitude rocket measurements of O_2 ($^1\Delta_g$) airglow, *Evans and Llewellyn* [1970] deduce O_3 local maximum values of 1-3 × 10^8 cm^{-3} (depending on time of day), occurring a little higher in altitude, ~88-90 km. *Noxon* [1982] presents the results of 10 years of O_2 ($^1\Delta_g$) airglow observations, and he too finds an 88 km secondary maximum of $\sim 4 \times 10^8$ cm^{-3} at high latitudes (twilight, winter solar maximum sun). Our model results do approximate these values with due allowance given for the varying circumstances of the observations. *Noxon* [1982] also finds that the O_3 column above 80 km increases from summer to winter by a factor of 3 at mid- to high latitudes, a trend that models (including our own) do not reproduce. It would be important to verify this observation by additional measurements.

The O_3 secondary maximum was first directly measured by *Hays and Roble* [1973], using occultations by the terrestrial atmosphere of ultraviolet stellar light as detected by the OAO 2 satellite, and by *Miller and Ryder* [1973], employing a rocket-borne solar occultation experiment. Both groups of observations show a high altitude bulge, but the structure is more clearly defined in the work of *Hays and Roble* [1973]. Their (nighttime) profiles show the O_3 peak typically at 83-85 km, varying between 6×10^7 and 3×10^8 cm^{-3} in magnitude. Our model peak value for midnight under the conditions of a summer solar minimum sun is $\sim 1.2 \times 10^8$ cm^{-3}, which compares well with the *Hays and Roble* [1973] mid-latitude summer solar maximum predawn peak value of 10^8 cm^{-3}. When computed with a solar maximum spectrum, the model secondary maximum is ~25% larger than at solar minimum. The altitude of the O_3 local minimum in the *Hays and Roble* [1973] data is at ~75 km, whereas our model local minimum is at ~78 km, not a serious difference considering the envelope of the observational profiles. The *Hays and Roble* [1973] profiles and our model results are in overall agreement between 60 and 95 km, the altitude range for which these authors expected the best retrievals from the satellite data. However, below 60 km, the gradient of the O_3 profile is a factor of 10 smaller than that calculated by most models (including our own) and observed by others (see later section in this paper). This is probably reflecting the breakdown in the retrieval scheme at low altitudes recognized by *Hays and Roble* [1973]. A major conclusion of theirs is that, in the altitude range of their observations, they see little change in O_3 during the night. The results of the diurnal calculations (see Figure 8) are consistent with this, except for a narrow altitude range near 80 km where a small nighttime variation is predicted to occur.

Later satellite stellar occultation observations of mesosphere/lower thermosphere O_3 were performed by *Riegler et al.* [1977], this time with the OAO 3 *Copernicus*. Their summer nighttime solar minimum equatorial measurements show the secondary maximum to be larger ($\sim 2.5 \times 10^8$ cm^{-3}) and higher (97 km) than our mid-latitude model values. The value for the density peak can be modified by changing environmental conditions (as has already been demonstrated in this paper), but the altitude is much higher than any of the previously obtained observations, including the equatorial results of *Hays and Roble* [1973]. In the lower mesosphere, the *Riegler et al.* [1977] O_3 densities are 2-3 times larger than expected from models and prior observations and are in direct conflict with the results of other techniques obtained close by in space and in time (*Gille et al.*, 1980*a*). However, a large ($\sim 6 \times 10^8$ cm^{-3}) and high (93 km) O_3 nighttime peak was measured recently at high latitudes by *Vaughan* [1982], using a rocket-borne lunar occultation technique.

By monitoring O_2 ($^1\Delta_g$) emission, the Solar Mesosphere Explorer (SME) measured O_3 to 90 km at 3 P.M. local time and only sometimes detected secondary maxima (*Thomas et al.*, 1983] as is expected from the model diurnal calculations for daytime. In mid-latitudes at winter solstice, *Thomas et al.* [1983] find the O_3 mixing ratios increasing continuously to 90 km from a local minimum at ~70 km, with the 90 km values being ~1-1.25 ppmv ($7\text{-}9 \times 10^7$ cm^{-3}). These values are more than a factor of 3 larger than our model results for this season. Significant day-to-day variability is seen at 90 km [*Barth et al.*, 1983], and their explanation concerns variability in the downward transport of active-O from the thermosphere. As already discussed in this paper, transport does affect O_3 at the mesopause, but temperature fluctuations can also produce similar effects (see the next section). However, the high mean values for O_3 at 90 km observed by the SME in the first 6 months of 1982 (~1 ppmv) and the large secondary maximum measured by *Vaughan* [1982] may be due to a more systematic change at the mesopause from the time of the early 1970's. There may have been a secular change in the H_2O abundance in the upper mesosphere; mesopause H_2O values of *Drummond and Mutlow* [1981] and *Bevilacqua et al.* [1983] are 2-3 times smaller than our model H_2O profile which was tuned to improve the model fit to the Aladdin

74 O_3 profile. A reduction in the local H_2O abundance would result in an almost proportionate increase in O_3. The H_2O distribution could change due to a reduction in H_2O at the stratopause or, as proposed by *Bevilacqua et al.* [1983], the upper mesosphere becoming stagnant leading to photolytic depletion of H_2O starting lower in the mesosphere than in our current model. So our basic model adjusted to match the Aladdin 74 observations may still be appropriate for that epoch, but recent observations may reflect the degree to which the atmosphere varies naturally, the subject of the next section of this paper.

In the context of the chemistry incorporated in our basic model, tested through comparisons with a number of observations, we can understand the origin of the O_3 secondary maximum. The O_3 maximum around 85 km results from a maximum in the production of O_3 (reactions (R13)-(R15)) at this altitude, as seen in Figure 3. Above 80 km, O_3 is a tracer for active-O. The concentration of the major form of active-O, atomic-O, is decreasing rapidly with decreasing altitude (and increasing atmospheric density) (Figure 9). The contrasting gradients of atomic-O and atmospheric density produce the peak in the production of O_3. As discussed in Paper I, the long lifetime of atomic-O in the thermosphere results in downward transport to the mesopause where there is a rapid enhancement of the conversion of active-O to O_2 (Figure 7). The lifetime of active-O has become short (Figure 2) without a proportionately increased source which would offset the effect of the extra loss. With decreasing altitude to 80 km, the extra reactivity of active-O is the result of the increasing OH abundance (Figure 13*c*), which catalyzes the active-O conversion to O_2 (Figure 4). Thus, ultimately the O_3 secondary maximum is tied to the presence and photochemistry of H_2O at the mesopause. The rapid decrease of OH with increasing altitude above 80 km results from the increasing photolysis of H_2O, leading to a sharp dropoff in the H_2O profile (Figure 14) and the consequent decrease in active-H production. The active-H produced is rapidly converted to H_2, from which little active-H can be derived (Figure 7). Moreover, the active-H that is present is predominantly atomic-H rather than OH. The depth of the local minimum at 80 km varies significantly as a function of time of day as discussed earlier in this paper. The subsequent increase in O_3 concentration with decreasing altitude through the mesosphere results from the increasing atmospheric density causing in turn an increase in the production of active-O from the photodissociation of O_2 (reactions (R1)-(R2)) and an increase in the ratio of O_3 to atomic-O. Throughout this lower altitude range, the OH concentration profile is relatively constant so active-H chemistry plays a less important role in affecting the shape of the O_3 profile.

Above the altitude of the local maximum in the O_3 density in the lower thermosphere, the O_3 concentration progressively decreases with increasing altitude, for example, as observed in the Aladdin 74 flight (see Figure 11). Although the basic model of this paper is able to reproduce the O_3 profile right above the mesopause, the calculated falloff with increasing altitude is very different than what was observed, in spite of the fact that the important species affecting the O_3 profile (equation (1)) are properly calculated (see Paper I). The difference between our model results and the Aladdin 74 observation is a factor of 2.5-7 at 100 km. In addition to the *Weeks et al.* [1978] Aladdin 74 daylight measurement of O_3 above the secondary maximum, other observations of O_3 in this altitude range have been made at night. The results of the basic model of this paper are 4.7 $\times 10^6$ and 4.2 $\times 10^3$ cm^{-3} for the O_3 densities at 100 and 110 km, respectively, at midnight. At a different season and phase of solar cycle, with variations in environmental factors, the model midnight value at 100 km could be higher by a factor of 5 and at 110 km higher by a factor of 50. The measurements of *Hays and Roble* [1973] of between 10^6 and 10^7 cm^{-3} for O_3 at 100 km can be accounted for by the model. However, the *Riegler et al.* [1977] values of 2 $\times 10^8$ and 2 $\times 10^7$ cm^{-3} at 100 and 110 km, respectively, and the *Vaughan* [1982] measurement of 6 $\times 10^7$ cm^{-3} at 100 km are not readily explained by our current model. One possibility is that the O_3 chemistry above 95 km may be different from that between 50 and 95 km. Further discussion of this point will appear in another paper.

NATURAL VARIABILITY OF OZONE

To improve the agreement between the O_3 profile measured in the Aladdin 74 program and model results generated for the purposes of intercomparison, a number of critical parameters were considered and modified within reasonable limits: chemical rate constants and the climatological factors of atmospheric composition, mass transport rates, and temperature field. Along with changing solar zenith angle that results in diurnal variations in the O_3 profile, natural fluctuations of environmental parameters will result in different O_3 distributions being observed. A good test of our model description of the O_3 chemistry would be to explain the natural variability of O_3 as reflected in the accumulation of O_3 measurements, much of which have been recently acquired by a variety of sensors in earth orbit.

In Table 3, we present a systematic summary of the sensitivity of O_3 to changes in various atmospheric parameters. There is no entry for the O_3 perturbation resulting from variability in vertical transport because of the difficulty in characterizing a change in a simple fashion, but a sense of this effect is presented earlier in this paper. The impact of the diurnal cycle in solar insolation was discussed from a theoretical point of view earlier in this paper; the model results will be compared with a number of recently obtained observations in the next section.

Variations in the solar illumination also result from seasonal changes in the mean solar illumination angle and from the 11-year cycle in the spectral output of the sun (the spectral changes of the 27-day solar cycle being similar but smaller in magnitude, as clearly measured by the Solar Mesosphere Explorer [*Rottman et al.*, 1982]). Sensitivity tests were run for these two cases and the results are in Table 3.

The reduction in solar illumination from summer to winter (mean zenith angle is increased) increases the daytime ozone level below 80 km because the photolytic source of active-H decreases proportionately more than the photolytic production of active-O or the photodissociation of O_3, the ratio of the last two remaining relatively constant (see Table 2). Above 80 km, the reduction in photolytic rate

constants has the opposite effect; O_3 decreases as a consequence of more H_2O at the mesopause and a decreased abundance (and downward flux) of atomic-O. These results assume that all other parameters, including temperature and transport parameters, will not change with season. However, at latitude 40°N, the mean December temperature is about 10 K less than the mean June value at 50 km altitude but is ~20 K warmer at 80 km (CIRA, 1972). This temperature variability enhances the summer to winter increase in O_3 in the lower mesosphere and can double the summer to winter reduction at 80 km (see Table 3). The additivity of the effects of variation in illumination and temperature is correct only when these changes are referred to the same pressure level in both seasons (see later discussion).

When the solar zenith angle is constant (fixed season) and the solar spectrum is changed from solar minimum to solar maximum, the calculations predict minimal change in mesospheric O_3, but an appreciable increase in O_3 at and above the mesopause. The altitude trend in the magnitude of the variation in summer shown in Table 3 is similar to that reported by *Garcia et al.* [1983]. *Brasseur et al.* [1983] calculate an increase throughout most of the summer mesosphere and also a smaller increase in the lower thermosphere than in *Garcia et al.* [1983] or our model. Although they are both two-dimensional calculations, *Brasseur et al.* [1983] find O_3 decreasing at the winter mesopause while *Garcia et al.* [1983] see minimal seasonal effects. Computations we have performed using a winter sun support the conclusions of *Garcia et al.* [1983].

The solar minimum to solar maximum increase in O_3 at the mesopause and in the lower thermosphere is a consequence of two effects [*Garcia et al.*, 1983; S. Solomon, private communication, 1983], tied to the increase in solar flux at Lyman α by almost a factor of 2, while at the same time solar flux longward of 180 nm changes very little [*Mount and Rottman*, 1981]. If the H_2O profile in the calculations were to be fixed, the increased photolysis of H_2O at Lyman α would result in less O_3. But the photolytic lifetime of H_2O is comparable to the time scale for replenishment by upward transport at and above the mesopause such that over the course of the 11-year solar cycle (or the 27-day cycle) the H_2O abundance will change, becoming lower at solar maximum as illustrated in Figure 5*b* of Paper I. In addition, at solar maximum, O_2 photodissociation and the downward flux of atomic-O increases. Because the atmosphere is optically thick at the Lyman α wavelength below the mesopause, the model predicts little change in the O_3 profile below 80 km over the course of either solar cycle. These conclusions are contrary to some earlier model calculations of the solar cycle effects on mesospheric O_3. The 11-year solar cycle computations of *DeBaets et al.* [1981] show large decreases in O_3 above 70 km at solar maximum. This result is probably because the H_2O profile was held constant for the comparison, although this detail is not addressed in the paper. Similarly, the 27-day solar cycle model calculations of *Frederick* [1977] show large negative changes in O_3 above ~65 km at the maximum of Lyman α emission. In this case, *Frederick* [1977] clearly states that the H_2O profile was left unchanged. Since the time scales for photolysis of H_2O and eddy diffusion transport are less than or about a few days below 100 km (see Figure 1 in Paper I), actually not much change in O_3 should be expected during the course of a 27-day cycle. To examine this point further, we did a 14-day calculation (diurnally averaged radiation field) using a solar maximum spectrum but starting at the basic model O_3 profile for solar minimum illumination. Minimal change ($\lesssim$1%) occurred below 80 km, but above there were increases in O_3 of 8% at 84 km, 28% at 90 km, and 16% at 100 km. Since the actual variation in the solar spectrum over a 27-day cycle is less than over the 11-year cycle, such changes in O_3 in a 14-day period would not be expected, but the trend is suggestive.

The sensitivity of the O_3 profile to the local values of H_2O and temperature has already been discussed at several points in this paper. The distribution of H_2O above the stratopause is very dependent on the upward transport from the stratosphere as represented in our model computations by the 40 km (lower) boundary condition entered for the H_2O mixing ratio. Table 3 shows the consequences of the different values used in our calculations. To enhance the ability of the calculations to reproduce the Aladdin 74 observations, the adopted temperature field was increased by 20 K. The effect of such a change is also summarized in Table 3. The enhanced sensitivity to variation in temperature at the stratopause and in the lower thermosphere is due to the increased importance of $O + O_3$ (reaction (R16)) to the loss of O_3 at these altitudes. Among the reactions to which O_3 is most sensitive, the activation energy of (R16) is one of the largest. The change in O_3 due to temperature fluctuations at a given altitude actually will be somewhat different from the values reported in Table 3 because at a specific altitude temperature and pressure are inversely correlated, leading to changes in photolytic rate constants. However, in the calculations reported in Table 3, the density profile has been held constant so that the indicated degree of variation roughly represents the sensitivity at the pressure associated with the stated altitude in the basic model. Measurements of the response of O_3 to temperature changes have been derived from an intercomparison of near simultaneous NIMBUS 4 observations of temperature and ozone abundance at the same pressure level and solar illumination angle (and therefore relatively unvarying photolytic rates) yielding the relation that $d(\ln[O_3])/d(1/T) \simeq$ 1000-1200 K at 0.9 mbar (~50 km, 45°S, September 5, 1970) [*Barnett et al.*, 1975]. Also with data from NIMBUS 4, an analysis of temperature and ozone variations at the stratopause at 60°N over a 12 month period in 1970-1971 yields an O_3 temperature sensitivity of 1062 K [*Krueger et al.*, 1980]. In our model, the sensitivity at 50 km (constant density) to temperature fluctuations occurring on time scales less than ~12 hours shows a covariance of ~1120 K. If all species, including long-lived ones such as H_2O, are allowed to relax to steady state with varying temperatures, the covariance increases to 1300 K.

Tuned for the circumstances of the Aladdin 74 measurements, our model results can also be compared with a larger group of mid-latitude O_3 observations if the variability of solar insolation and climatological parameters (Table 3) is kept in mind. Indeed, the variety of conditions under which the available measurements have been made can be used to check the predictions of our model. The discussion of model results and O_3 observations at the mesopause is

presented elsewhere in this paper. However, most measurements have been of the lower mesosphere, which is fortuitous for the purposes of this comparison since solar cycle effects are expected to be minimal and the daytime variability due to changing solar zenith angle is only ~13% at 50 km, 25% at 60 km, increasing to 41% at 70 km in our model. The variability of seasonally changing illumination and local H_2O abundance potentially can add variance from model predictions (see Table 3) of 16% at 50 km, 18% at 60 km, increasing to 46% at 70 km. The exact value of the local temperature is the parameter in the lower mesosphere that can have the biggest impact on the observed value of O_3, adding a potential variability factor of 34% at 50 km, 22% at 60 km, and 26% at 70 km for a 20 K change in temperature.

Since the temperature profile of our basic model has been modified to improve the agreement with observations at a particular epoch, it is best to compare model computations utilizing a standard temperature profile with the larger set of published mid-latitude measurements (with the focus on northern hemisphere data obtained since 1971). As all model and observational profiles smoothly decrease from the stratopause to 70 km, selected altitudes can reliably represent more detailed profiles. Resulting from a calculation using the temperature profiles of Paper I, the diurnally averaged (approximately mean daylight) solar minimum mid-latitude summer O_3 values are 3.4 ppmv (8.0×10^{10} cm^{-3}) at 50 km, 2.1 ppmv (2.7×10^{10} cm^{-3}) at 55 km, 1.3 ppmv (9.1×10^{9} cm^{-3}) at 60 km, 0.78 ppmv (3.1×10^{9} cm^{-3}) at 65 km, and 0.39 ppmv (7.9×10^{8} cm^{-3}) at 70 km. *Krueger and Minzner* [1976] determined a mean ozone profile, nominally for 45°N latitude, by averaging the results of a variety of measurement techniques (balloon-, rocket-, and satellite-borne sensors) to obtain annual mean daylight values of 3.1 (±17%) ppmv at 50 km, 1.1 (±34%) ppmv at 60 km, and 0.31 (±57%) ppmv at 70 km, which are in very good agreement with our model results. It is interesting to note the increase in the uncertainty in the mean value with increasing altitude, varying as expected if just diurnal changes are considered. Most relevant for comparison with our model tuned for the epoch of Aladdin 74 are the mid-latitude summer measurements obtained by several satellite experiments the next summer (July 1975) when the solar activity was still at a minimum. The NIMBUS 6 LRIR instrument measured daytime O_3 values for 38°N of ~3.3 ppmv at 50 km and ~1.5 ppmv at 60 km [*Gille*, 1980; *Gille et al.*, 1980*c*). Mid-latitude O_3 values from the OSO 8 ultraviolet solar occultation (sunset) experiment obtained during the same time period are ~2-2.2 × 10^{10} cm^{-3} at 55 km, ~8.5 × 10^{10} cm^{-3} at 60 km, and ~2.5 × 10^{9} cm^{-3} at 65 km. *Ogawa and Watanabe* [1981] report O_3 densities for late summer at 31°N acquired during a 9 year (1970-1979) series of rocket ultraviolet solar absorption measurements; the mean values are ~7 × 10^{10} cm^{-3} at 50 km, ~8 × 10^{9} cm^{-3} at 60 km, and ~8 × 10^{8} cm^{-3} cm at 70 km. The agreement between the model results and observational values is very good, considering that most of these observations have measurement uncertainties of at least 10%.

During late fall 1979 (solar maximum), two series of rocket-borne solar and lunar ultraviolet absorption experiments were carried out to determine detailed vertical O_3 profiles at different times of the day. The *Lean* [1982] series was launched at 38°N latitude over a 2-week period. At a more northerly latitude a few weeks earlier, *Vaughan* [1982] had several flights in a 24-hour period. A discussion of the diurnal variability observed by these experiments is saved for the next section; at this point we will compare the model results with representative points on the vertical profiles. The *Lean* [1982] noontime value for O_3 at 50 km was ~5.5 × 10^{10} cm^{-3}, and the sunset (χ = 87°) values were ~6 × 10^{10} cm^{-3} at 50 km, ~6 × 10^{9} cm^{-3} at 60 km, and ~2.5 × 10^{8} cm^{-3} (±50%) at 70 km. The midmorning values (χ = 70°) observed by *Vaughan* [1982] were 6 × 10^{10} cm^{-3} at 50 km and 6 × 10^{9} cm^{-3} at 60 km. The corresponding values of our model, calculated with a solar maximum sun at equinox at 34°N latitude and a March 1 background atmosphere (see next section) are at 9 A.M. (χ = 64°) 7.1 × 10^{10} cm^{-3} (50 km) and 7.5 × 10^{9} cm^{-3} (60 km), at noon 6.4 × 10^{10} cm^{-3} (50 km), and at sunset (χ = 88°) 7.3 × 10^{10} cm^{-3} (50 km), 7.8 × 10^{9} cm^{-3} (60 km), and 3.2 × 10^{8} cm^{-3} (70 km). Our computations are systematically 15-20% larger than the late fall observations. However, this can be explained by seasonal differences in the background atmosphere (the pressure at a given altitude in fall is lower than in spring, resulting in larger photolytic rate constants and slower three-body reactions) which result in spring O_3 values being larger than fall values by about 20% in both model calculations and observations [*Prather*, 1981].

Observations by the Solar Mesosphere Explorer (SME) satellite of scattered solar ultraviolet [*Rusch et al.*, 1983*a*] and infrared airglow [*Thomas et al.*, 1983] during the first winter of the recent onset of low solar activity find values for mid-latitude O_3 in the afternoon (local time) of ~3 ppmv at 50 km, ~0.8 ppmv at 60 km, and ~0.25 ppmv at 70 km. The results of our model run with a winter sun (set to the epoch of the *Anderson et al.* [1980] flight) and a January 1 background atmosphere (CIRA, 1972) are 2.8 ppmv at 50 km, 1.1 ppmv at 60 km, and 0.28 ppmv at 70 km, in good agreement with the observations considering the measurement uncertainties and the degree of variability in the observations [*Barth et al.*, 1983].

Systematic changes in O_3 due to seasonal variability of key climatological parameters are implicit in the differences in the O_3 profiles (models and observations) for the different seasons just discussed. Using data from different experiments to determine secular variations will probably introduce errors due to systematic differences between the experiments, so the following discussion will emphasize comparison with single instrument data sets. As discussed by *Prather* [1981], model seasonal trends must be referred to a constant pressure or altitude, whichever is appropriate for the comparison observational data set, since the results in the two cases are different. In agreement with his model computations, we find that, upon using the appropriate background model atmosphere and solar illumination, at a specific altitude the O_3 density in winter is 25-45% less (O_3 mixing ratio 15-30% less) than in summer, between 50 and 90 km. On the other hand, at a constant pressure level (to which the constant density calculations reported in Table 3 are very similar) there is a summer to winter increase of 28% near 1 mbar, ~20% increase near 0.1 mbar (where there is little seasonal temperature variation), and a 73% decrease near 0.001 mbar. Intercomparisons of rocket mea-

surements reveal seasonal variations usually at a given altitude. The summer to winter decrease in the lower mesosphere calculated in our model and that of *Prather* [1981] is seen in the ROCOZ (rocket ozone project) results at 38°N from 1976 to 1979 [*Wright et al.*, 1978; *Krueger and Wright*, 1979]. On the other hand, *Ogawa and Watanabe* [1981] find at 60 and 70 km at 31°N latitude a summer to winter increase of a factor of 2, which is not supported by the observations of others nor can it be reproduced by any current model. Satellite experiments often measure O_3 relative to pressure. At 1 mbar at mid-latitudes, the NIMBUS 4 BUV data acquired over a 2-year period (1970-1972) and the NIMBUS 7 SBUV data obtained in 1978 and 1979 show a 40% increase in winter O_3 values [*McPeters*, 1980; *Frederick et al.*, 1983].

Probably the most detailed measurements of seasonal changes in O_3 come from the SME satellite program [*Barth et al.*, 1983]. Obtained continuously during the first 6 months of 1982, the SME results for O_3 at 48 km at mid-latitudes clearly show an inverse correlation between the O_3 abundance and seasonal variation in temperature [*Barth et al.*, 1983] which was measured simultaneously [*Rusch et al.*, 1983*b*]. At 48 km, the summer to winter increase in O_3 is ~17% in both hemispheres, while at 64 km the SME measures a summer to winter decrease of ~33% in the northern hemisphere and ~8% in the southern hemisphere and at 90 km a decrease in the mean seasonal value of $\lesssim$18% in both hemispheres [*Barth et al.*, 1983]. The exact magnitude of these changes depends on whether the variation refers to a constant altitude surface, as was the case just quoted, or a constant pressure surface, as seen in the 40°S results of *Thomas et al.* [1983] where the summer to winter increase is 40% at 1 mbar (~48 km) (cf. BUV/SBUV results) and 20% at 0.1 mbar (~64 km) and a decrease of ~20% at 0.001 mbar (~90 km). Acquired with a different instrument on the SME, the results of *Rusch et al.* [1983*a*] show little seasonal change at 0.1 mbar at 45°S latitude.

Except for two instances, the various observations of seasonal trends in O_3 in the lower mesosphere are in reasonably good agreement with each other and with models. As discussed before, the *Ogawa and Watanabe* [1981] measurements cannot be explained. The SME results at 48 km (constant altitude) showing a summer to winter increase [*Barth et al.*, 1983] are not consistent with other observations and model calculations referred to a constant altitude. The difference could result from small errors in determining the SME altitude scale. However, in the lower thermosphere (90 km), the SME-measured summer to winter O_3 decrease [*Barth et al.*, 1983; *Thomas et al.*, 1983] is significantly smaller than in the model. One factor that has not been included in the model estimates of seasonal variation is the possibility of systematic changes in atmospheric motion. Either as the result of summer to winter hemispheric transport [*Garcia and Solomon*, 1983] or as a consequence of seasonal variation in eddy diffusion [*Lindzen*, 1981], the upward flow of H_2O to the mesopause may be enhanced in summer relative to the winter, diminishing the contrast in mesopause H_2O values (that occur due to seasonal changes in solar zenith angle) and the consequent variation in O_3. The interhemisphere motions will enhance the downward transport of atomic O from the thermosphere in the winter and thereby contribute to higher O_3 values at the mesopause and in the lower thermosphere than our current model would produce.

The model prediction of little systematic variation in O_3 in the lower mesosphere due to solar cycle effects is consistent with several different observations. The 9 years of rocket measurements accumulated by *Ogawa and Watanabe* [1981] show no variation correlated with the phase of the solar cycle. Indeed, the mid-latitude winter measurements obtained by OGO 4 during an earlier period of heightened solar activity (late 1960's) [*London et al.*, 1977; *Clayson et al.*, 1981] and the results obtained during the most recent time of maximum solar output [*Remsberg et al.*, 1981; *Sundararamen et al.*, 1981; *WMO*, 1981] are in good agreement with the measured solar minimum winter values quoted earlier. Again, one must keep in mind the potential for error when making comparisons between data acquired by different experiments.

DIURNAL VARIATION OF OZONE

Earlier in this paper the chemical interactions resulting in the diurnal variation of ozone in the mesosphere and lower thermosphere were discussed and the results of the basic model illustrated in Figure 8. This diurnal variation can play an important role in upper atmospheric phenomena. The magnitude of the variation is diagnostic of key processes affecting the ozone distribution. Therefore, a detailed comparison between models and observations of the diurnal variation is an additional and important test of our theoretical picture of ozone chemistry.

The Aladdin 74 observations, the measurements for which the diurnal results of the basic model are most appropriate, yield only a little information concerning diurnal changes, daylight values in post-dawn and afternoon periods. The chemiluminescent sonde data sets obtained during these two time periods show few differences between 50 and 60 km, consistent with the daytime model results. In Figure 4 of *Weeks et al.* [1978], the ultraviolet absorption data obtained in early morning are compared with the afternoon data of the airglow photometer between 74 and 84 km. Both measured O_3 profiles show structure, but, given the indicated error bars, the reality of any of the features and of any diurnal variations is not clear. Our diurnal calculation (see Figure 8) predicts that the local minimum in O_3 in the mesopause should be enhanced in the post-dawn period compared with late afternoon, but the Aladdin 74 data is not sufficiently precise to check this theoretical result.

The NIMBUS 6 LRIR experiment had the ability to observe O_3 during both day and night and preliminary analyses [*Gille et al.*, 1980*b*] showed a day-to-night increase of ~20(±10)% in the altitude range 56-66 km, but little diurnal change at 50 km, similar to what is predicted by our model. In a more refined investigation employing LRIR measurements, *Anderson et al.* [1981] obtained an internally consistent set of data for O_3 at 50°S latitude on December 19-21, 1975. Being from the solar minimum period and at the southern hemisphere summer solstice, these observational results are directly comparable with the model calculations shown in Figure 8. At 50 km, *Anderson et al.* [1981] report O_3 night (χ = 97°) to day (χ = 35°) ratios of 1.1 at 50 km increasing to 2-3 at 67 km (the

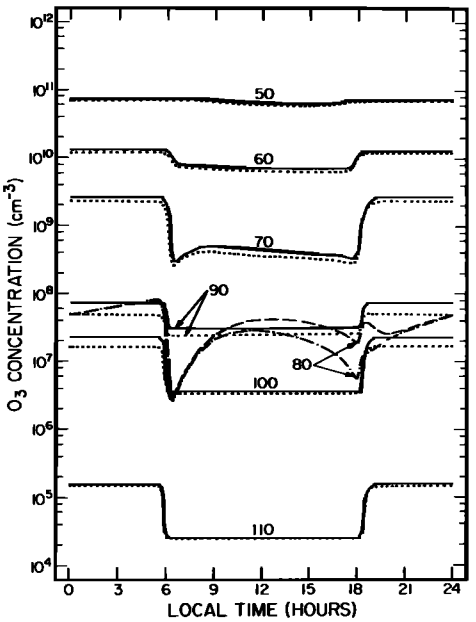

Fig. 16. The diurnal variation of O_3 calculated for a near-spring equinox sun at solar maximum at 34°N latitude. Results are shown for altitudes 50, 60, 70, 80, 90, 100, and 110 km. The concentration of H_2O at 40 km is 7 ppmv (solid and dashed lines) or 10 ppmv (dotted and dash-dotted lines). In the latter case, $k_{30} = 0$ to maximize the abundance of active-H species near the mesopause.

operational ceiling of the LRIR instrument). For similar zenith angles, our corresponding model values are 1.1 at 50 km and 3.2 at 67 km.

Most useful for detecting the diurnal changes of O_3 are sets of data obtained by the same measurement technique, preferably the same instrument, covering the whole mesosphere and/or including many points in the diurnal cycle. Appreciating the importance of doing such measurements, a number of groups have recently reported the results of experiments that satisfy the aforementioned criterion. Since all of this observational work was conducted during the recent solar maximum time period, we performed diurnal calculations for conditions of solar maximum flux [*Mount and Rottman*, 1981], close to spring equinox at 34°N latitude, using a 30°N March 1 model atmosphere (temperature, total density, N_2 density versus altitude) from CIRA (1972) and an appropriate thermospheric model from *Jacchia* [1977]. The kinetic rate constants, 40 km H_2O boundary condition of 7 ppmv, and eddy diffusion coefficients of the basic model were also used in these computations. We show in Figure 16 the equinox model O_3 concentrations for a 24-hour period. The results of a calculation with similar solar illumination have been reported by *Rusch and Liu* [1981] and are roughly similar to Figure 16. As might be expected from a combination of different seasonal solar illumination and model atmosphere parameters (see Table 3), the noontime O_3 densities of this equinox model are within ±20% of our basic model results below 70 km, in which altitude range solar cycle effects are not significant.

The O_3 measurements reported by *Lean* [1982] are a compilation of rocket results acquired over a 2-week period, October-November 1979 at 38°N latitude. Since these flights occurred at different local times (one of them at night [*Lean*, 1983]), taken together the results can provide a picture of the diurnal variation of O_3. *Lean* [1982] adjusts the new O_3 values to account for probable environmental changes occurring over the 2-week period that would affect the O_3 measurements. The observational results for the change from night (0527 LST) to day (~noon local time) are -12% (50 km), -45% (60 km), and -84% (70 km), the equinox model results being very similar (-15, -45, -83%, respectively). The O_3 values were also observed to decrease from midmorning to early-afternoon by about 10-15% at 50 and 60 km, model results again being similar. Interestingly, the sunset observations in the mesosphere are less than the nighttime values because the altitude range is still well illuminated.

The *Vaughan* [1982] rocket measurements of O_3 diurnal variation come from flights that all occurred within a 24 hour period (night: 0200 LST, dawn: 0600 LST, morning: 0930 LST). The background atmosphere is not expected to have changed as much as occurred in the *Lean* [1982] rocket series. Since the rocket launches were at 57°N in early October of 1979, the solar insolation will be similar to or even a little less than the equinox model with which the observations will be compared. Little diurnal variation was observed below 54 km. Above that altitude, there was an observed decrease from night to morning of ~39% at 60 km, the model predicting a 42% decrease. From nighttime to dawn ($\chi = 95.5°$) *Vaughan* [1982] observed a factor of 10 decrease in O_3 at 70 km and a similar decrease above 80 km. The model does not show such changes over a similar time span. Since the 2 A.M. flight also observed an unusually large secondary maximum, the data from this particular flight may conceivably be erroneous or conditions were such as to invalidate the comparison with our equinox model.

Resulting from ground-based radio observations of atmospheric ozone emission, the diurnal O_3 measurements of *Wilson and Schwartz* [1981] have poor spatial resolution. However, these observations present the most detailed picture of the temporal variation of ozone yet published since data were obtained continuously throughout several full diurnal cycles. *Wilson and Schwartz* [1981] present their data in three different ways. In each case there may be errors due to the difficulties inherent in accurately measuring radio emission and interpreting such data in terms of vertical distribution. In Figure 2 of *Wilson and Schwartz* [1981], vertical profiles for O_3 for noon and midnight derived from their data are shown. They find very little difference between day and night values (within their error bars of ±70%) below 60 km, consistent with model calculations. The night-to-day ratio increases above 60 km to very large values. These O_3 distributions are derived from the observed emission spectra shown in their Figure 1 where it is seen that the area of the central channel, sensitive to the total O_3 column above 70 km, increases from noon to midnight by a factor of 10^3. On the other hand, contradicting this result are the data plotted in their Figure 4 which, averaged over a 10-day period, are the brightness temperature differences between their observing channels, each difference pairing being sensitive to the O_3 column in somewhat different altitude ranges above the stratopause. The results shown in their Figure 4 display only a 150% increase in column O_3 above ~70 km compared with the 10^3 increase of their Figures 1 and 2. The observations

presented in their Figures 1 and 2 are only from one particular day, so the mean behavior may be better represented by the average results in their Figure 4. Their Figures 1 and 2 further may be considered to have large errors because the results of other diurnal measurements (and model calculations) already discussed in our paper show changes of a factor of 10 or less. The O_3 profiles shown in their Figure 2 retrieved from their Figure 1 may also be in error in that the mixing ratio at 50 km is ~1 ppmv and at 60 km 0.2 ppmv, significantly lower than the range of O_3 values measured in the lower mesosphere by a variety of techniques, all of which are very close to each other independent of a variety of fluctuations in environmental factors.

It seems that the results in Figure 4 of *Wilson and Schwartz* [1981], which are an average of 10 days of observation, hold the most promise for containing useful information, with which model computations can be compared. The solar illumination adopted for the equinox model calculation (the diurnal results appearing in our Figure 16) was specifically chosen to simulate the circumstances of these radio observations. Since the *Wilson and Schwartz* [1981] Figure 4 results are each convolutions over several scale heights, we smoothed our model values by the difference weighting functions in Figure 3 of *Wilson and Schwartz* [1981] to generate comparable diurnal profiles. The results of the model smoothing and the observed brightness temperature differences were each normalized to the minimum point of the 24-hour period and are presented as the percentage increase above the minimum point in Figure 17. Figure 5 of *Wilson and Schwartz* [1981] is a temporally smoothed version of their data shown in Figure 17. The convolved diurnal variations for 48-68 km and 58-76 km are similar in the model and observations (within the noise limits). However, the convolved model variation for 76-114 km needs to be reduced by a factor of 4 in order to match the measurements. Why the observational result for the highest altitude range could be in error by as much as a factor of 4 is as follows. The minimum value for the brightness temperature difference is only 1% of the observed signals being differenced. Considering the noise in the recorded spectra as represented by the noise in the brightness temperature differences shown in Figure 4 of *Wilson and Schwartz* [1981], one cannot exclude the possibility of an unremoved nonlinear baseline that varied by $\gtrsim$1% per channel (W. Wilson, private communication, 1982). This would introduce errors in the night-to-day variation as plotted in Figure 17, the largest error occurring in the 76-114 km calculation where the differences are smallest. Furthermore, our calculations for O_3 at the mesopause earlier in this paper have been shown to be consistent with other observations.

It is interesting to note from the structure in the smoothed model diurnal variabilities (Figure 17) that in each case the altitude to which the convolved profile is most sensitive is not the one at the peak of the weighting function (such would be the case only if O_3 were uniformly distributed in altitude). The 76-114 km smoothed profile clearly shows the structure of O_3 variability in a narrow range at the mesopause, far below the peak of the weighting function.

When the 76-114 model convolution is reduced by a factor of 4, the observed variability in O_3 is reproduced by the model. In particular, the model shows a night-to-day decrease an hour before ground sunrise as a result of the sphericity of the terrestrial atmosphere. Both the symmetry around noon in daylight O_3 values in the lower mesosphere and the asymmetry in the upper mesosphere as seen in the radio data are reproduced by the model calculations. When appropriately scaled to match the gross night-to-day variation, the smoothed model result for 76-114 km shows that some structure due to the unusual mesopause variability (see Figure 16) is not washed out but is comparable to the noise level of the observational results. Thus, an observational measurement sensitive enough to prove or disprove the existence of this temporal structure predicted by a number of models, including our own, does not yet exist.

The observations available to date are fairly well reproduced by model calculations. It is clear that the diurnal variability of O_3 will change with differences in key environmental factors. A comparison of Figures 8 and 16 shows that the varying length of day due to changing season will result in very dissimilar diurnal profiles. Another factor explored by M. Prather (private communication, 1980) and *Vaughan* [1982] is the impact of different amounts of active

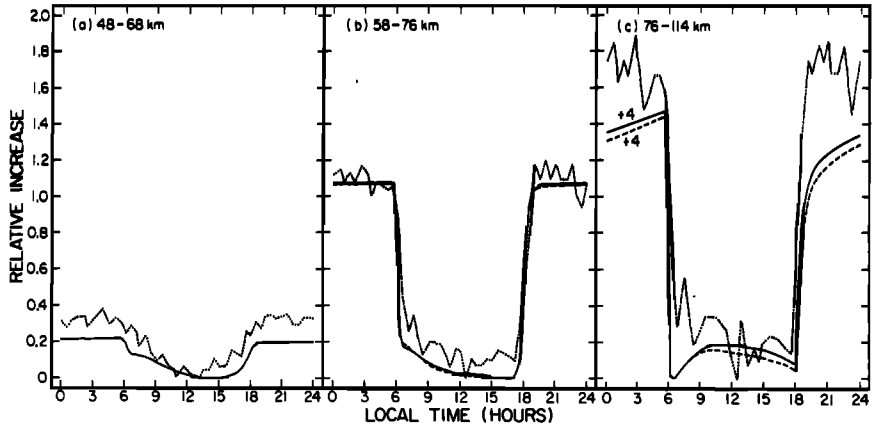

Fig. 17. The results of the calculations described in Figure 16 smoothed by the weighting functions displayed in Figure 3 of *Wilson and Schwartz* [1981]. The solid line is the 7 ppmv model and the dashed line is the 10 ppmv model. The dotted lines are the measured brightness temperature differences from Figure 4 of *Wilson and Schwartz* [1981]. In the case of the 76-114 km convolution (*c*), the model values are reduced by a factor of 4 (see text).

hydrogen (as controlled by the H_2O abundance). We performed an equinox diurnal calculation which maximized active-H by increasing the H_2O boundary condition at 40 km to 10 ppmv and diminishing the active-H to inactive-H conversion by setting the rate constant for (R30) ($H + HO_2 \rightarrow H_2 + O_2$) to zero. The resulting diurnal profiles are shown in Figure 16 and the smoothed profiles (as in *Wilson and Schwartz* [1981]) are displayed in Figure 17. The difference in the O_3 diurnal variability due to different amounts of active-H that we have calculated is qualitatively similar to the previously published calculations of others. Given the signal-to-noise of the data, the *Wilson and Schwartz* [1981] measurements were not sensitive to the precise H_2O profile at the time of the observations.

Comparison With Other Models

Since the models of ozone in the mesosphere and lower thermosphere that have been published within the past 10 years all have the same important reactions, variability in the results must arise from differences in computational techniques, solar illumination calculations, rate constants, and/or environmental parameters. A survey of this earlier theoretical work in light of our current model will further illustrate the sensitivity of our results to the approach and parameters we have adopted. A comparison of results at certain specific altitudes should be most instructive. At 50 km, there is little variation due to diurnal or solar cycle changes in the solar illumination and only a weak sensitivity to different values adopted for H_2O at the stratopause. The situation is similar at 60 km, except for the slight diurnal variation between day and night. Thus, variability in the model results for the lower mesosphere will be a consequence mostly of different rate constants being used. On the other hand, the results of the different models at the secondary maximum near 80 km will be interesting to compare since O_3 at this altitude is very reflective of climatological variables used in the computations in addition to the adopted rate constants. One point that simplifies the intercomparison is that the O_3 values at noon and midnight at 80 km are very similar, although the values at other times are very different. A set of parameters not frequently reported is the adopted atmospheric temperature profile. While use of different standard atmospheres might result in changes in the O_3 calculations of as much as 50%, we will discuss in this section possible sources of differences between models of greater than 100%.

Hunt [1971, 1973] demonstrated the impact on the ozone profile due to the presence of mesospheric water. His ozone densities are systematically a factor of 2-4 larger than later calculations, but it is impossible to identify a single cause of this difference because all of his key rate constants are different from ours. For one thing, his lower boundary condition (at 60 km) for H_2O is 5 ppmv, whereas our H_2O mixing ratio at the same altitude is ~7 ppmv. The drier mesosphere will result in increased O_3 (up to 40%, see Table 3) at all altitude levels. Moreover, because of the adopted rate constants, the key active-H species for catalytic destruction of active-O, OH, is significantly less in *Hunt* [1971, 1973] than in our basic model, also causing an increase in active-O. The rate constant for three-body recombination forming O_3 is also larger in the aforementioned work. Differences in the computation of the photolytic rate constants enhance the O_3.

The results of *Thomas and Bowman* [1972] are well suited for comparison with our calculations since theirs is explicitly a mid-latitude model. Their mesosphere is rather dry (~3 ppmv at 60 km). However, the reported O_3 densities at 60 km are surprisingly similar to ours, and the mesopause secondary maximum is smaller than our value, contrary to what is expected. Their O_3 can be understood as resulting from the fact that the increased efficiency of three-body O_3 formation, low local H_2O, and, at 60 km, a larger value for the ratio of key photolytic rate constants ($J_{1+2}/J_{3+4}J_{5+6}^{1/2}$) are offset by a smaller value for the ratio of key kinetic rate constants [$(k_{23}/k_{17}k_{18})^{1/2}$]. At the secondary maximum, near 80 km, both the photolytic rate constant ratio ($J_{1+2}^2/J_{3+4}J_{5+6}$) and the kinetic rate constant ratio ($k_{30}/k_{18}k_{28}$) are lower, thus explaining the reduced O_3. In general, the critical rate constants are factors of 2-5 different from what we are using, sometimes larger, sometimes smaller, necessitating the approach of comparing the two models using the simplified analytical expressions.

The *Whitten and Turco* [1974] and *Koshelev* [1976] models are very similar in choice of rate constants. The O_3 densities in both papers are larger than our values by factors of 2-10. This is true at the mesopause where the development of the secondary maximum is slight and, depending on the choice of the eddy diffusion profile, occurs above 90 km. The high O_3 profile is the result of a significant minimization of active-H destruction of active-O resulting from a very fast value for $OH + HO_2$ ($k_{23} = 2 \times 10^{-10}$ cm^{-3}; 2.3 times larger than our k_{23}) conversion of active-H back to inactive-H. The OH concentration is further suppressed by extra slow cycling from HO_2 to OH via the reaction $O + HO_2$ ($k_{18} = 1 \times 10^{-11}$ cm^{-3} s^{-1}; 6 times smaller than our value).

The model of *Moreels et al.* [1977] uses rate constants more similar to ours and also has an abundance of H_2O at 50 km (6 ppmv) close to the value we have. Although there are some differences in rate constant values, at 50 km the ratios of the important rate constants are very similar to our ratios such that their calculated O_3 concentration is in good agreement with our value. Although their O_3 secondary maximum is at about the same altitude as in our model, it is about a factor of 3 larger. This may be most directly due to a mesopause H_2O concentration 4 times smaller than ours, resulting from a combination of different eddy diffusive transport and the H_2O photolysis rate constants they report being larger than our values.

With the top boundary near 80 km, *Logan et al.* [1978] and *Prather* [1981] cannot properly calculate O_3 at the mesopause, thus explaining why no structure is seen in the O_3 profiles near 80 km. With rate constants close to what we have employed, their models yield O_3 profiles in the lower mesosphere in very good agreement with our results. In both cases, the abundance of H_2O in the lower mesosphere is ~5 ppmv.

Although of recent vintage, the *Keneshea et al.* [1979] model uses older values for the key rate constants compared with other contemporary models and our own work. Active-H is suppressed by a fast value for $OH + HO_2$ and a particularly slow value for $O + HO_2$, coupled with a drier lower mesosphere of ~4 ppmv. This can explain their

values for O_3 in the lower mesosphere being larger than ours by factors of 1.5-3. By 80 km, the *Keneshea et al.* [1979] profile is very similar to our own (magnitude and altitude of secondary maximum); the values of the rate constants of particular importance at the mesopause are closer to what we have. However, no details are presented in that paper concerning the photolytic rate constant values, so further intercomparison is not possible.

Computed O_3 densities larger than ours occur in the recent models of *Crutzen and Solomon* [1980] at 80 km and of *Wang et al.* [1981] throughout the mesosphere. In the former work, the use of the *Hack et al.* [1978, 1979] branching ratios for H + HO_2 (our (R30)-(R32)), would contribute to this result by depleting active-H at the mesopause more than would occur with the current rate constant values. In the latter paper, a slow value for O + HO_2 (our k_{18}) is used, which would tend to produce an O_3 increase.

The multidimensional model of *Garcia and Solomon* [1983] is a contemporary of our own work. They present a mid-latitude annual average for the O_3 vertical profile. In this case we would expect from Table 3 that their lower mesosphere O_3 would be somewhat higher than ours, but actually it is lower by 20%. Their mesopause O_3 shows more structure than our own. However, from the experience of fitting a particular measured O_3 profile, we know that small variations in the rate constants adopted would result in the profile of *Garcia and Solomon* [1983]. The values of key climatological variables — H_2O, temperature, transport — play a significant role in determining the O_3 profile so that differences in these variables will also introduce differences between the results of different models when compared in as much detail as we have done in this section. A recent application of the *Garcia and Solomon* [1983] model involves a comparison between photochemical calculations and the vertical distribution of O_3 as measured from 50 to 95 km by the SME [*Solomon et al.*, 1983]. The model results are systematically lower than the observations throughout this altitude range. Their results better fit the mesopause measurements than do ours, but this probably arises from their adoption of a drier mesosphere. Both models could easily match the upper mesosphere SME results if reduced H_2O abundances on the order of the *Bevilacqua et al.* [1983] profile were adopted, a point *Solomon et al.* [1983] also mention. The *Solomon et al.* [1983] calculations fit the SME results least well in the lower mesosphere, while our model results for the appropriate circumstances of the observations fall a little on the high side in this altitude range. They propose one solution to the deficiency that involves modifying the photolysis rates. Interestingly, the adoption of our photodissociation rate constants would result in an increase in their calculated results (S. Solomon, private communication, 1983), the differences between the models arising from the use of different radiative transfer parametrizations in the wavelength range dominated by the complex Schumann-Runge bands of O_2 (our techniques discussed in Paper I and *Allen and Frederick* [1982]). This is a clear demonstration of the sensitivity of model conclusions to the exact details of the computations.

During the past decade, modeling techniques have been refined and rate constant values standardized. In this section, we have considered our model in light of its predecessors. Differences between the earlier work and the results presented in this paper can be attributed to the adoption of different values for the important parameters, rather than any inconsistencies in the chemical model itself.

CONCLUSIONS

A sizeable body of mid-latitude mesosphere/lower thermosphere ozone measurements has been acquired within the last 15 years by a wide range of observing techniques. We attempt in this paper to provide a theoretical understanding of the variety of phenomena illustrated by these sets of data. We are aided in this analysis by simple analytical expressions that can well describe the ozone abundances over much of the day at the various altitude levels. Particular attention is paid to the detailed ozone profile from the Aladdin 74 rocket flights, which we found to be reproduced by model calculations when adjustments are made to key parameters within the range of their known uncertainty. This model can explain, in general, the observed natural variability of lower mesosphere ozone due to changes in environmental factors, but assumptions about the values of some critical climatological parameters always need to be made. The interesting, but less frequently measured, secondary maximum near the mesopause is shown to arise from the coupling of active-hydrogen and active-oxygen chemistry. The abundance of ozone at the mesopause seems to undergo significant variation, which may be the result of secular variation in the dynamics of that altitude range. We find that the measured ozone profile above 100 km cannot be matched by calculations. Since only a few reactions in the current model are important in that altitude range and the magnitude of these processes are well constrained, new reactions need to be considered.

Thus, key chemical cycles involving oxygen and hydrogen atoms that are important to ozone in the mesosphere and lower thermosphere and also in the stratosphere have been verified to a large degree. Currently, the observed variability of ozone can be ascribed to changes in climatological variables. However, this satisfying picture of our understanding of ozone above the stratopause is not truly accurate. Even though very few parameters need to be specified to calculate the ozone abundance, our knowledge of the correct values to use is surprisingly poor. The uncertainties in the laboratory measurements of the key rate constants are too large for the type of comparisons that need to be made. For example, the recently revised quantum yields for H_2O photodissociation at Lyman α [*Slanger and Black*, 1982] result in a doubling of J_5 at 100 km (but little change below 70 km) and in a decrease in J_6 by a factor of 6 throughout the atmosphere (relative to the values reported in Table 1 and shown in Figure 10). The consequences of these changes can be understood in terms of the discussion in our paper. Active-O is reduced by 50% at the mesopause and by 10% at 70 and 90 km. The reduction in O_3 is similar to that of active-O at and below the mesopause; the reduction is somewhat larger in the lower thermosphere (90 km, 35%; 100 km, 10%). The decrease in J_6 reduces the rate of conversion of H_2O to H_2, resulting in an enhancement of H_2O of 20% at the mesopause and above. The consequent reduction in H_2 (cf. Figure 14) is 21% at 50 km, 32% at 60 km, 64% at 70 km, and 35-45% at and above 80

km. As expected from equation (13), the atomic H values change very little in the mesosphere but double in the lower thermosphere. Being the dominant active-H species in the mesosphere, OH reflects the changes in J_5 and is increased by 13% at 70 km and 78% at 80 km (and in the lower thermosphere, 88% at 90 km and 57% at 100 km). The abundance of HO_2 is coupled to that of OH (equation (5)), such that the changes in OH are echoed in HO_2. The reaction (R27) involving two molecules of HO_2 produces H_2O_2 and, as a result, there is a consequent amplification of the increases in HO_2 seen in the H_2O_2 profile. These changes in the abundances of the trace species, however, do not affect the general trends in the O_3 response to temporal and climatological variability.

To refine our investigations of upper atmospheric ozone, there is an additional need to acquire simultaneously and cospatially with ozone data the full set of important environmental factors. The solar illumination is reasonably well defined for a given pressure level at a specific local time. The temperature at each pressure level for which ozone is measured also needs to be determined. The critically important water profile, from which the catalytically significant active hydrogen species are derived, and the nature of atmospheric transport could be obtained by simultaneous measurements of other easily observable species, in particular, water itself and carbon monoxide. An example of an observing program designed to acquire a sufficient complement of measurements to test our understanding of ozone chemistry is the Solar Mesosphere Explorer (SME) satellite [*Thomas et al.*, 1980; *Barth*, 1981; *Barth et al.*, 1983]. However, the SME obtains the necessary set of measurements only near the stratopause. Future experiments need to be developed to extend the program of complementary measurements through the mesosphere to the complex and interesting mesopause region. In addition, the apparent deficiency of model ozone above 95 km (which we shall discuss further in another paper) needs to be verified by more measurements of ozone in this altitude range.

Briefly outlined in the introduction to this paper is the importance of ozone to the physics and chemistry of the upper atmosphere in a variety of ways. If an understanding of the "normal" variability of ozone is achieved, "abnormal" ozone values can be recognized and the fact that the atmosphere is being "unusually" perturbed also can then be recognized. In this way, new correlations of terrestrial atmospheric behavior with other phenomena may be identified. Furthermore, an understanding of ozone chemistry and related processes permits better analyses of the future response of the atmosphere to a variety of anthropogenic modifications.

Acknowledgments. The many conversations we have had with S. Solomon have been of significant help in writing this paper. We also gratefully acknowledge the variety of assistance received from D. Anderson, G. Anderson, T. Clancy, W. DeMore, J. Gille, D. Hunten, F. Kaufman, L. Keyser, M. Leu, J. Logan, D. Muhleman, M. Prather, S. Sander, P. Schwartz, J. Waters, and W. Wilson. This research was supported by NASA grant NAGW 413 and JPL49-649-20320-0-3270 to the California Institute of Technology. Contribution number 3876 from the Division of Geological and Planetary Sciences, California Institute of Technology.

REFERENCES

Ackerman, M., Ultraviolet solar radiation related to mesospheric processes, in *Mesospheric Models and Related Experiments*, edited by G. Fiocco, pp. 149-159, D. Reidel, Hingham, Mass., 1971.

Allen, M., and J. E. Frederick, Effective photodissociation cross sections for molecular oxygen and nitric oxide in the Schumann-Runge bands, *J. Atmos. Sci., 39*, 2066-2075, 1982.

Allen, M., Y. L. Yung, and J. W. Waters, Vertical transport and photochemistry in the terrestrial mesosphere and lower thermosphere (50-120 km), *J. Geophys. Res., 86*, 3617-3627, 1981.

Anderson, D. E., P. D. Feldman, E. P. Gentieu, and R. R. Meier, The UV dayglow, 2, LY alpha and LY beta emissions and the H distribution in the mesosphere and thermosphere, *Geophys. Res. Lett., 7*, 529-532, 1980.

Anderson, G. P., J. C. Gille, P. L. Bailey, and S. Solomon, LRIR observations of diurnal ozone variation in the mesosphere, in *Proceedings Quadrennial International Ozone Symposium*, edited by J. London, pp. 580-585, International Ozone Commission, Boulder, Col., 1981.

Anderson, J. G., Rocket-borne ultraviolet spectrometer measurement of OH resonance fluorescence with a diffusive transport model for mesospheric photochemistry, *J. Geophys. Res., 76*, 4634-4652, 1971.

Atreya, S. K., T. M. Donahue, W. E. Sharp, B. Wasser, J. F. Drake, and G. R. Riegler, Ultraviolet stellar occultation measurement of the H_2 and O_2 densities near 100 km in the earth's atmosphere, *Geophys. Res. Lett., 3*, 607-610, 1976.

Baker, K. D., J. C. Ulwick, C. R. Philbrick, and R. Picard, Mid-latitude measurements of atmospheric minor species, *EOS Trans. AGU, 63*, 1048, 1982.

Banks, P. M., and G. Kockarts, *Aeronomy, Part B*, Academic, New York, 1973.

Barnett, J. J., J. T. Houghton, and J. A. Pyle, The temperature dependence of the ozone concentration near the stratopause, *Q. J. R. Meteorol. Soc., 101*, 245-257, 1975.

Barth, C. A., Solar Mesosphere Explorer to study ozone, *Nature, 293*, 259-260, 1981.

Barth, C. A., D. W. Rusch, R. J. Thomas, G. H. Mount, G. J. Rottman, G. E. Thomas, R. W. Sanders, and G. M. Lawrence, Solar Mesosphere Explorer: Scientific objectives and results, *Geophys. Res. Lett., 10*, 237-240, 1983.

Bates, D. R., and M. Nicolet, The photochemistry of atmospheric water vapor, *J. Geophys. Res., 55*, 301-327, 1950.

Battaner, E. and R. Rodrigo, Meospheric O_3, H and H_2O at high latitudes: a theoretical model, *Planet. Space Sci., 29*, 819-823, 1981.

Bevilacqua, R. M., P. R. Schwartz, J. M. Bologna, D. L. Thacker, J. J. Olivero, and C. J. Gibbons, An observational study of water vapor in the mid-latitude mesosphere using ground-based microwave techniques, *J. Geophys. Res., 88*, 8523-8534, 1983.

Brasseur, G., P. DeBaets, and A. DeRudder, Solar variability and minor constituents in the lower thermosphere and in the mesosphere, *Space Sci. Rev., 34*, 377-385, 1983.

Carver, J. H., H. P. Gies, T. I. Hobbs, B. R. Lewis, and D. G. McCoy, Temperature dependence of the molecular oxygen photoabsorption cross section near H Lyman alpha line, *J. Geophys. Res., 82*, 1955-1960, 1977.

Chamberlain, J. W., *Theory of Planetary Atmospheres: An Introduction to Their Physics and Chemistry*, Academic, New York, 1978.

Chang, J. S., and W. H. Duewer, Modeling chemical processes in the stratosphere, *Ann. Rev. Phys. Chem., 30*, 443-469, 1979.

Chanin, M.-L., and A. Hauchecorne, Lidar observation of gravity and tidal waves in the stratosphere and mesosphere, *J. Geophys. Res., 86*, 9715-9721, 1981.

CIAP, *The Natural Stratosphere of 1974, Monogr. 1, DOT-TST-75-51*, Climatic Impact Assessment Program, Department of Transportation, Washington, D. C., 1975.

Cicerone, R. J., and J. L. McCrumb, Photodissociation of isotopically heavy O_2 as a source of atmospheric O_3, *Geophys. Res. Lett., 7*, 251-254, 1980.

Clayson, M. H., J. London, and G. P. Anderson, The global distribution of stratospheric ozone from OGO-4 BUV observations, in *Proceedings Quadrennial International Ozone Symposium*, edited

by J. London, pp. 558-564, International Ozone Commission, Boulder, Col., 1981.
Crutzen, P. J., and S. Solomon, Response of mesospheric ozone to particle precipitation, *Planet. Space Sci., 28*, 1147-1153, 1980.
DeBaets, P., G. Brasseur, and P. C. Simon, Chemical response of the middle atmosphere to solar variations, *Solar Phys., 74*, 349-353, 1981.
Deguchi, S., and D. O. Muhleman, Mesospheric water vapor, *J. Geophys. Res., 87*, 1343-1346, 1982.
DeMore, W. B., and Y. L. Yung, Catalytic processes in the atmospheres of Earth and Venus, *Science, 217*, 1209-1213, 1982.
DeMore, W. B., L. J. Stief, F. Kaufman, D. M. Golden, R. F. Hampson, M. J. Kurylo, J. J. Margitan, M. J. Molina, and R. T. Watson, Chemical Kinetics and Photochemical Data for Use in Stratospheric Modeling, Eval. 4, *JPL Publ. 81-3*, Jet Propul. Lab., Calif. Inst. of Tech., Pasadena, Calif., 1981.
DeMore, W. B., R. T. Watson, D. M. Golden, R. F. Hampson, M. Kurylo, C. J. Howard, M. J. Molina, and A. R. Ravishankara, Chemical Kinetics and Photochemical Data for Use in Stratospheric Modeling, Eval. 5, *JPL Publ. 82-57*, Jet Propul. Lab., Calif. Inst. of Tech., Pasadena, Calif., 1982.
Dickinson, P. H. G., W. C. Bain, L. Thomas, E. R. Williams, D. B. Jenkins, and N. D. Twiddy, The determination of the atomic oxygen concentration and associated parameters in the lower ionosphere, *Proc. R. Soc. London Ser. A, 369*, 379-408, 1980.
Drummond, J. R., and C. T. Mutlow, Satellite measurements of H_2O fluorescence in the mesosphere, *Nature, 294*, 431-432, 1981.
Evans, W. F. J., and E. J. Llewellyn, Molecular oxygen emissions in the airglow, *Ann. Geophys., 26*, 167-178, 1970.
Evans, W. F. J., and E. J. Llewellyn, Atomic hydrogen concentrations in the mesosphere and the hydroxyl emissions, *J. Geophys. Res., 78*, 323-326, 1973.
Evans, W. F. J., D. M. Hunten, E. J. Llewellyn, and A. Vallance Jones, Altitude profile of the infrared atmospheric system of oxygen in the dayglow, *J. Geophys. Res., 73*, 2885-2896, 1968.
Farmer, C. B., O. F. Raper, B. D. Robbins, R. A. Toth, and C. Muller, Simultaneous spectroscopic measurements of stratospheric species: O_3, CH_4, CO, CO2, N2O, H_2O, HCl, and HF at northern and southern mid-latitudes, *J. Geophys. Res., 85*, 1621-1632, 1980.
Frederick, J. E., Chemical response of the middle atmosphere to changes in the ultraviolet solar flux, *Planet. Space Sci., 25*, 1-4, 1977.
Frederick, J. E., Influence of gravity wave activity on lower thermospheric photochemistry and composition, *Planet. Space Sci., 27*, 1469-1477, 1979.
Frederick, J. E., Seasonal variations in high-latitude ozone and metastable molecular oxygen emissions: A theoretical interpretation, *J. Geophys. Res., 85*, 1611-1617, 1980.
Frederick, J. E., Photochemical processes induced by a major warming of the upper atmosphere: Variations in mesospheric trace constituents, *J. Geophys. Res., 86*, 3148-3152, 1981*a*.
Frederick, J. E., Radiative-photochemical response of the mesosphere to dynamical forcing, *J. Geophys. Res., 86*, 5224-5230, 1981*b*.
Frederick, J. E., and R. D. Hudson, Atmospheric opacity in the Schumann-Runge bands and the aeronomic dissociation of water vapor, *J. Atmos. Sci., 37*, 1088-1098, 1980.
Frederick, J. E., and J. E. Mentall, Solar irradiance in the stratosphere: implications for the Herzberg continuum absorption of O_2, *Geophys. Res. Lett., 9*, 461-464, 1982.
Frederick, J. E., F. T. Huang, A. R. Douglass, and C. A. Reber, The distribution and annual cycle of ozone in the upper stratosphere, *J. Geophys. Res., 88*, 3819-3828, 1983.
Froidevaux, L., and Y. L. Yung, Radiation and chemistry in the stratosphere: Sensitivity to O_2 absorption cross sections in the Herzberg continuum, *Geophys. Res. Lett., 9*, 854-857, 1982.
Garcia, R. R., and S. Solomon, A numerical model of the zonally-averaged dynamical and chemical structure of the middle atmosphere, *J. Geophys. Res., 88*, 1379-1400, 1983.
Garcia, R. R., S. Solomon, R. G. Roble, and D. W. Rusch, A numerical study of the response of the middle atmosphere to the 11-year solar cycle, submitted to *J. Geophys. Res.*, 1983.
Gille, J. C., Ozone distributions by infrared limb scanning: Preliminary results from the LRIR, in Proceedings NATO Advanced Study Institute on Atmospheric Ozone: Its Variation and Human Influences, edited by A. C. Aikin, pp. 103-121, *FAA-EE-80-20*, U.S. Dept. of Transp., Washington, D. C., 1980.
Gille, J. C., G. P. Anderson, and P. L. Bailey, Comparison of near coincident LRIR and OAO-3 measurements of equatorial night ozone profiles, *Geophys. Res. Lett., 7*, 525-528, 1980*a*.
Gille, J. C., P. L. Bailey, and J. M. Russell, Temperature and composition measurements from the l.r.i.r. and l.i.m.s. experiments on NIMBUS 6 and 7, *Phil. Trans. R. Soc. London Ser. A, 296*, 205-218, 1980*b*.
Gille, J. C., P. L. Bailey, R. A. Craig, F. B. House, and G. P. Anderson, Sounding the stratosphere and mesosphere by infrared limb scanning from space, *Science, 208*, 397-399, 1980*c*.
Hack, N., H. Gg. Wagner, and K. Hoyermann, Reaktionen von wasserstoffatomen mit hydroperoxylradikalen, I, Bestimmung der spezikischen geschwindigkeits- konstanten der reaktionskanale, *Ber. Bunsenges. Phys. Chem., 82*, 713-719, 1978.
Hack, W., A. W. Preuss, H. Gg. Wagner, and K. Hoyermann, Reaktionen von wasserstoffatomen mit hydroperoxylradikalen, II, Bestimmung der geschwindigkeitskonstanten der bruttoreaktion, *Ber. Bunsenges. Phys. Chem., 83*, 212-217, 1979.
Hampson, R. F., Chemical kinetics and photochemical data sheets for atmospheric reactions, *FAA-EE-80-17*, U.S. Dept. of Transp., Washington, D. C., 1980.
Hauchecorne, A., and M.-L. Chanin, A mid-latitude ground-based lidar study of stratospheric warmings and planetary wave propagation, *J. Atmos. Terr. Phys., 44*, 577-583, 1982.
Hauchecorne, A., and M.-L. Chanin, Mid-latitude lidar observations of planetary waves in the middle atmosphere during the winter of 1981-1982, *J. Geophys. Res., 88*, 3843-3849, 1983.
Hays, P. B., and R. G. Roble, Observation of mesospheric ozone at low latitudes, *Planet. Space Sci., 21*, 273-279, 1973.
Herman, J. R., The response of stratospheric constituents to a solar eclipse, sunrise, and sunset, *J. Geophys. Res., 84*, 3701-3710, 1979.
Herman, J. R., and J. E. Mentall, O_2 absorption cross sections (187-225 nm) from stratospheric solar flux measurements, *J. Geophys. Res., 87*, 8967-8975, 1982.
Hudson, R. D., Critical review of ultraviolet photoabsorption cross sections for molecules of astrophysical and aeronomic interest, *Rev. Geophys. Space Phys., 9*, 305-406, 1971.
Hudson, R. D., Absorption cross sections of stratospheric molecules, *Can. J. Chem., 52*, 1465-1478, 1974.
Hudson, R. D. (ed.), Chlorofluoromethanes and the Stratosphere, *NASA RP-1010*, 1977.
Hudson, R. D., and E. I. Reed (eds.), The Stratosphere: Present and Future, *NASA RP-1049*, 1979.
Hunt, B. G., A diffusive-photochemical study of the mesosphere and lower thermosphere and the associated conservation mechanisms, *J. Atmos. Terr. Phys., 33*, 1869-1892, 1971.
Hunt, B. G., A generalized aeronomic model of the mesosphere and lower thermosphere including ionospheric processes, *J. Atmos. Terr. Phys., 35*, 1755-1798, 1973.
Hunten, D. M., Vertical transport in atmospheres, in *Atmospheres of Earth and the Planets*, edited by B. M. McCormac, pp. 59-72, D. Reidel, Hingham, Mass., 1975.
Hunten, D. M., and T. M. Donahue, Hydrogen loss from the terrestrial planets, *Ann. Rev. Earth Planet. Sci., 4*, 265-292, 1976.
Hunten, D. M., and D. F. Strobel, Production and escape of terrestrial hydrogen, *J. Atmos. Sci., 31*, 305-317, 1974.
Jacchia, L. G., Thermospheric temperature, density and composition: New models, *SAO Spec. Rep. 375*, Smithsonian Inst., Cambridge, Mass., 1977.
Johnston, H. S., and J. Podolske, Interpretation of stratospheric photochemistry, *Rev. Geophys. Space Phys., 16*, 491-519, 1978.
Kaufman, F., L. X. Qiu, and U. C. Sridharan, Radical-radical and atom-radical reactions of HO_2, paper presented at Seventh International Symposium Gas Kinetics, Royal Society of Chemistry of Great Britain, Gottingen, West Germany, 1982.
Keneshea, T. J., S. P. Zimmerman, and C. R. Philbrick, A dynamic model of the mesosphere and lower thermosphere, *Planet. Space Sci., 27*, 385-401, 1979.
Keyser, L. F., Kinetics of the reaction $O + HO_2 \rightarrow OH + O_2$ from 229 to 372 K, *J. Phys. Chem., 86*, 3439-3446, 1982.
Kita, D., and W. E. Sharp, Atomic hydrogen in the upper mesosphere, *EOS Trans. AGU, 63*, 896, 1982.
Klais, O., P. C. Anderson, and M. J. Kurylo, A reinvestigation of

the temperature dependence of the rate constant for the reaction $O + O_2 + M \rightarrow O_3 + M$ (for M = O_2, N_2, and Ar) by the flash photolysis resonance fluorescence technique, *Int. J. Chem. Kinet., 12*, 469-490, 1980.

Ko, M. K. W., and N. D. Sze, Effect of recent rate data revisions on stratospheric modeling, *Geophys. Res. Lett., 10*, 341-344, 1983.

Koshelev, V. V., Diurnal and seasonal variations of oxygen, hydrogen and nitrogen components at heights of mesosphere and lower thermosphere, *J. Atmos. Terr. Phys., 38*, 991-998, 1976.

Krueger, A. J., and R. A. Minzner, A mid-latitude ozone model for the 1976 U.S. Standard Atmosphere, *J. Geophys. Res., 81*, 4477-4481, 1976.

Krueger, A. J., and D. U. Wright, Some results from rocket ozone (ROCOZ) soundings at Wallops Island, Va., *EOS Trans. AGU, 60*, 268, 1979.

Krueger, A. J., B. Guenther, A. J. Fleig, D. F. Heath, E. Hilsenrath, R. McPeters, and C. Prabnakara, Satellite ozone measurements, *Phil. Trans. R. Soc. London, Ser. A, 296*, 191-204, 1980.

Lean, J. L., Observation of the diurnal variation of atmospheric ozone, *J. Geophys. Res., 87*, 4973-4980, 1982.

Lean, J. L., UV rocket spectroscopy measurement of the nighttime ozone distribution, *J. Geophys. Res., 88*, 1468-1474, 1983.

Lin, C. L., and M. T. Leu, Temperature and third-body dependence of the rate constant for the reaction $O + O_2 + M \rightarrow O_3 + M$, *Int. J. Chem. Kinet., 14*, 417-434, 1982.

Lindzen, R. S., Turbulence and stress owing to gravity wave and tidal breakdown, *J. Geophys. Res., 86*, 9707-9714, 1981.

Liu, S. C., and T. M. Donahue, The aeronomy of hydrogen in the atmosphere of the earth, *J. Atmos. Sci., 31*, 1118-1136, 1974*a*.

Liu, S. C., and T. M. Donahue, Realistic model of hydrogen constituents in the lower atmosphere and escape flux from the upper atmosphere, *J. Atmos. Sci., 31*, 2238-2242, 1974*b*.

Logan, J. A., M. J. Prather, S. C. Wofsy, and M. B. McElroy, Atmospheric chemistry: Response to human influence, *Phil. Trans. R. Soc. London, Ser. A, 290*, 187-234, 1978.

London, J., Radiative energy sources and sinks in the stratosphere and mesosphere, in Proceedings NATO Advanced Study Institute on Atmospheric Ozone: Its Variation and Human Influences, edited by A. C. Aiken, pp. 703-721, *FAA-EE-80-20*, U.S. Dept. of Transp., Washington, D. C., 1980.

London, J., J. E. Frederick, and G. P. Anderson, Satellite observations of the global distribution of stratospheric ozone, *J. Geophys. Res., 82*, 2543-2556, 1977.

McPeters, R. D., The behavior of ozone near the stratopause from two years of BUV observations, *J. Geophys. Res., 85*, 4545-4550, 1980.

Miller, D. E., and P. Ryder, Measurement of the ozone concentration from 55 to 95 km at sunset, *Planet. Space Sci., 21*, 963-670, 1973.

Millier, F., A. Vidal-Madjar, J. Guidon, and R. G. Roble, Ozone number density profiles in the lower mesosphere as determined by the French experiment on board OSO-8, *Geophys. Res. Lett., 6*, 863-865, 1979.

Millier, F., B. A. Emery, and R. G. Roble, OSO-8 lower mesospheric ozone number density profiles, in *Proceedings Quadrennial International Ozone Symposium*, edited by J. London, pp. 572-579, International Ozone Commission, Boulder, Col., 1981.

Moreels, G., G. Megie, A. Vallance Jones, and R. L. Gattinger, An oxygen-hydrogen atmospheric model and its application to the OH emission problem, *J. Atmos. Terr. Phys., 39*, 551-570, 1977.

Mount, G. H., and G. J. Rottman, The solar spectral irradiance 1200-3184 Å near solar maximum: July 15, 1980, *J. Geophys. Res., 86*, 9193-9198, 1981.

Mount, G. H., G. J. Rottman, and J. G. Timothy, The solar spectral irradiance 1200-2550 Å at solar maximum, *J. Geophys. Res., 85*, 4271-4274, 1980.

National Academy of Sciences, *Solar-Terrestrial Research for the 1980's*, Washington, D. C., 1981.

Nicolet, M., Aeronomic reactions of hydrogen and ozone, in *Mesospheric Models and Related Experiments*, edited by G. Fiocco, pp. 1-51, D. Reidel, Hingham, Mass., 1971.

Nicolet, M., The chemical equations of stratospheric and mesospheric ozone, in Proceedings NATO Advanced Study Institute on Atmospheric Ozone: Its Variation and Human Influences, edited by A. C. Aiken, pp. 823-864, *FAA-EE-80-20*, U.S. Dept. of Transp., Washington, D. C., 1980.

Noxon, J. F., A global study of O_2 ($^1\Delta_g$) airglow: Day and twilight, *Planet. Space Sci., 30*, 545-557, 1982.

Offermann, D., V. Friedrich, P. Ross, and U. von Zahn, Neutral gas composition measurements between 80 and 120 km, *Planet. Space Sci., 29*, 747-764, 1981.

Ogawa, T., and T. Watanabe, Summary of the mesospheric ozone measurements during 1970-1979 in Japan, in *Proceedings Quadrennial International Ozone Symposium*, edited by J. London, pp. 520-525, International Ozone Commission, Boulder, Col., 1981.

Prather, M. J., Ozone in the upper stratosphere and mesosphere, *J. Geophys. Res., 86*, 5325-5338, 1981.

Remsberg, E. E., J. M. Russell, L. L. Gordley, J. C. Gille, and P. L. Bailey, The validation of LIMS ozone profiles using correlative rocket, ECC, and Dobson data sets, in *Proceedings Quadrennial International Ozone Symposium*, edited by J. London, pp. 190-195, International Ozone Commission, Boulder, Col. 1981.

Riegler, G. R., S. K. Atreya, T. M. Donahue, S. C. Liu, B. Wasser, and J. F. Drake, UV stellar occultation measurements of nighttime equatorial ozone, *Geophys. Res. Lett., 4*, 145-148, 1977.

Rottman, G. J., Rocket measurements of the solar spectral irradiance during solar minimum, 1972-1977, *J. Geophys. Res., 86*, 6697-6705, 1981.

Rottman, G. J., C. A. Barth, R. J. Thomas, G. H. Mount, G. M. Lawrence, D. W. Rusch, R. W. Sanders, G. E. Thomas, and J. London, Solar spectral irradiance, 120 to 190 nm, October 13, 1981-January 3, 1982, *Geophys. Res. Lett., 9*, 587-590, 1982.

Rusch, D. W., and S. C. Liu, The effects of recent solar flux measurements and water vapor dissociation calculations on mesospheric chemistry, in *Proceedings Quadrennial International Ozone Symposium*, edited by J. London, pp. 869-875, International Ozone Commission, Boulder, Col., 1981.

Rusch, D. W., G. H. Mount, C. A. Barth, G. J. Rottman, R. J. Thomas, G. E. Thomas, R. W. Sanders, G. M. Lawrence, and R. S. Eckman, Ozone densities in the lower mesosphere measured by a limb scanning ultraviolet spectrometer, *Geophys. Res. Lett., 10*, 241-244, 1983*a*.

Rusch, D. W., G. H. Mount, J. M. Zawodny, C. A. Barth, G. J. Rottman, R. J. Thomas, G. E. Thomas, R. W. Sanders, and G. M. Lawrence, Temperature measurements in the earth's stratosphere using a limb scanning visible light spectrometer, *Geophys. Res. Lett., 10*, 261-264, 1983*b*.

Schmidlin, F. J., Temperature inversions near 75 km, *Geophys. Res. Lett., 3*, 173-176, 1976.

Schurgers, M., and K. W. Welge, Absorptionskoeffizient von H_2O und N_2H_4 Zwischen 1200 and 2000 Å, *Z. Naturforsch. A., 23*, 1508-1510, 1968.

Slanger, T. G., and G. Black, Photodissociative channels at 1216 Å for H_2O, NH_3, and CH_4, *J. Chem. Phys., 77*, 2432-2437, 1982.

Solomon, S., E. E. Ferguson, D. W. Fahey, and P. J. Crutzen, On the chemistry of H_2O, H_2 and meteorite ions in the mesosphere and lower thermosphere, *Planet. Space Sci., 30*, 1117-1126, 1982.

Solomon, S., D. W. Rusch, R. J. Thomas, and R. S. Eckman, Comparison of mesospheric ozone abundances measured by the Solar Mesosphere Explorer and model calculations, *Geophys. Res. Lett., 10*, 249-252, 1983.

Sridharan, U. C., L. X. Qiu, and F. Kaufman, Kinetics and product channels of the reactions of HO_2 with O and H atoms at 296 K, *J. Phys. Chem., 86*, 4569-4574, 1982.

Sundararaman, N., T. Perry, W. Gurkin, E. Jackson, B. Horton, J. Lean, E. Llewellyn, B. Solheim, W. F. J. Evans, B. H. Subbaraya, S. Lal, T. Ogawa, T. Watanabe, E. Hilsenrath, and A. Krueger, International ozone rocketsonde intercomparison, in *Proceedings Quadrennial International Ozone Symposium*, edited by J. London, pp. 421-422, International Ozone Commission, Boulder, Col., 1981.

Thomas, G. E., C. A. Barth, E. R. Hansen, C. W. Hord, G. M. Lawrence, G. H. Mount, G. J. Rottman, D. W. Rusch, A. I. Stewart, R. J. Thomas, J. London, P. L. Bailey, P. J. Crutzen, R. E. Dickinson, J. C. Gille, S. C. Liu, J. F. Noxon, and C. B. Farmer, Scientific objectives of the Solar Mesosphere Explorer mission, *Pure Appl. Geophys., 118*, 591-615, 1980.

Thomas, L. and M. R. Bowman, The diurnal variations of hydrogen and oxygen constituents in the mesosphere and lower thermosphere, *J. Atmos. Terr. Phys., 34*, 1843-1858, 1972.

Thomas, R. J., and R. A. Young, Measurement of atomic oxygen and related airglows in the lower thermosphere, *J. Geophys. Res., 86*, 7389-7393, 1981.

Thomas, R. J., C. A. Barth, G. J. Rottman, D. W. Rusch, G. H. Mount, G. M. Lawrence, R. W. Sanders, G. E. Thomas, and L. E. Clemens, Ozone density distribution in the mesosphere (50-90 km) measured by the SME limb scanning infrared spectrometer, *Geophys. Res. Lett., 10*, 245-248, 1983.

Trainor, D. W., D. O. Ham, and F. Kaufman, Gas phase recombination of hydrogen and deuterium atoms, *J. Chem. Phys., 58*, 4599-4609, 1973.

Trinks, H., and K. H. Fricke, Carbon dioxide concentrations in the lower thermosphere, *J. Geophys. Res., 83*, 3883-3886, 1978.

Trinks, H., D. Offermann, U. von Zahn, and C. Steinhauer, Neutral composition measurements between 90- and 220-km altitude by rocket-borne mass spectrometer, *J. Geophys. Res., 83*, 2169-2176, 1978.

Vaughan, G., Diurnal variation of mesospheric ozone, *Nature, 296*, 133-135, 1982.

Wang, P. H., G. K. Yue, A. Deepak, and R. J. Kurzeja, A model study of the diurnal variation of mesospheric O_3, in *Proceedings Quadrennial International Ozone Symposium*, edited by J. London, pp. 876-883, International Ozone Commission, Boulder, Col., 1981.

Watanabe, K., Ultraviolet absorption processes in the upper atmosphere, *Adv. Geophys., 5*, 153-221, 1958.

Waters, J. W., J. J. Gustincic, P. N. Swanson, and A. R. Kerr, Measurement of upper atmospheric H_2O emission at 183 GHz, in *Atmospheric Water Vapor*, edited by A. Deepak, T. D. Wilkerson, and L. H. Ruhnke, pp. 229-240, Academic, New York, 1980.

Weeks, L. H., R. E. Good, J. S. Randhawa, and H. Trinks, Ozone measurements in the stratosphere, mesosphere, and lower thermosphere during Aladdin 74, *J. Geophys. Res., 83*, 978-982, 1978.

Whitten, R. C. and R. P. Turco, Perturbations of the stratosphere and mesosphere by aerospace vehicles, *AIAA J., 12*, 1110-1117, 1974.

Wilson, W. J., and P. R. Schwartz, Diurnal variations of mesospheric ozone using millimeter-wave measurements, *J. Geophys. Res., 86*, 7385-7388, 1981.

World Meteorological Organization, The Stratosphere 1981: Theory and Measurements, *Rep. 11*, WMO Global Ozone Res. and Monitoring Proj., Geneva, Switzerland, 1981.

Wright, D. U., A. J. Krueger, and G. M. Foster, Rocket ozone sounding network data, *NASA TM-69365*, 1978.

M. Allen, J. I. Lunine, and Y. L. Yung, Division of Geological and Planetary Sciences, California Institute of Technology, Pasadena, CA 91125.

(Received June 13, 1983;
revised December 5, 1983;
accepted December 5, 1983.)